mRNA reading frame maintenance during eukaryotic ribosome translocation

Nemanja Milicevic, Lasse Jenner, Alexander Myasnikov, Marat Yusupov, Gulnara Yusupova

mRNA reading frame maintenance during eukaryotic ribosome translocation

Nemanja Milicevic[1], Lasse Jenner[1], Alexander Myasnikov[2], Marat Yusupov[1] & Gulnara Yusupova[1,*]

[1] Institute of Genetics and Molecular and Cellular Biology, CNRS UMR7104, INSERM U1258, University of Strasbourg, 67400 Illkirch, Strasbourg, France.

[2] Dubochet Center for Imaging (DCI), EPFL, Lausanne, Switzerland.

Abstract

One of the most critical steps of protein synthesis is coupled translocation of messenger and transfer RNAs required to advance the mRNA reading frame by one codon. In eukaryotes, translocation is accelerated and its fidelity is maintained by elongation factor 2 (eEF2)[1,2]. Currently, only a few snapshots of eukaryotic ribosome translocation have been reported[3-5]. Here we report ten high-resolution cryo-EM structures (up to 1.97 Å) of the elongating eukaryotic ribosome bound to the full translocation module consisting of messenger RNA, peptidyl-tRNA and deacylated tRNA, seven of which also contained ribosome-bound, naturally modified eEF2. This study recapitulates mRNA-tRNA$_2$-growing peptide module progression through the ribosome, from the earliest states of eEF2 translocase accommodation until the very late stages of the process, and reveals an intricate network of interactions preventing the slippage of the translational reading frame. We demonstrate how the accuracy of eukaryotic translocation relies on eukaryote-specific elements of the 80S ribosome, eEF2 and tRNAs. Our findings shed light on the mechanism of translation arrest by the anti-fungal eEF2-binding inhibitor, sordarin. We also propose that the sterically constrained environment imposed by diphthamide, a conserved eukaryotic post-translational modification in eEF2, not only stabilizes correct Watson-Crick codon-anticodon interactions but may also uncover erroneous peptidyl-tRNA, and therefore contribute to higher accuracy of protein synthesis in eukaryotes.

Main

During protein synthesis, messenger RNA (mRNA) and transfer RNAs (tRNA) must be rapidly translocated through the ribosome to advance the translational reading frame by one codon. The process is susceptible to errors, of which the most severe is shifting of the translational reading frame of mRNA, causing incorrect reading of succeeding codons. The key question is how the eukaryotic ribosome couples mRNA and tRNA translocation during protein synthesis, while securing the integrity of weak codon-anticodon interactions and thus preventing frameshifting. Many bacterial ribosome intermediates of translocation have been structurally analyzed employing both X-ray crystallography and cryo-EM[6-11], however, insights into eukaryotic translocation complexes have been hindered by low-to-intermediate resolution[3-5]. The higher complexity of the eukaryotic 80S ribosome, with approximately 40 % higher molecular mass than its prokaryotic counterpart, and a minimum mass of 3.3 MDa in yeast and plants, hampered the high-resolution structural study of eukaryotic translocation, arguably the most complex operation of protein synthesis. Apart from being more sophisticated in terms of function and regulation[12-14], an increasing number of genetic and biochemical studies report that the eukaryotic translational apparatus relies to a large extent on unique post-transcriptional modifications of ribosomal RNA (rRNA) and tRNAs, as well as kingdom-specific elongation factors, which actively contribute to the accuracy of protein synthesis.

In eukaryotes, the process of translocation is ensured by a five-domain GTP-ase, elongation factor 2 (eEF2). Eukaryotic eEF2 and archaeal aEF2, contain a unique and strictly conserved post-translationally modified histidine residue located at the tip of domain IV, named diphthamide, and shown to contribute to translation accuracy[1,2]. Its biosynthesis pathway requires the action of at least seven enzymes and even involves non-canonical radical enzyme chemistry. Diphthamide in human eEF2 is a target of at least two virulent toxins that inactivate eEF2 by ADP-ribosylation and cause lethal effects[1,15,16]. By failing to respond to high oxidative stress, mammalian cells lacking diphthamide are more sensitive to cell death[17]. Moreover, the loss of diphthamide can lead to several neurodegenerative diseases[18,19] and render human cells hypersensitive to Tumor Necrosis Factor-mediated apoptosis[20]. A recent crystal structure of the *Saccharomyces cerevisiae* ribosome translocation intermediate revealed that domain IV of eEF2 and diphthamide engaged in an extensive stabilization network with the codon–anticodon duplex

in an early state of translocation[3], however the role of diphthamide in other translocation phases remained unanswered.

We determined ten high-resolution cryo-EM structures (up to 1.97 Å) of elongating eukaryotic *S. cerevisiae* ribosome bound to the full translocation module consisting of messenger RNA, peptidyl-tRNA and deacylated tRNA, seven of which also contained ribosome-bound *S. cerevisiae* eEF2. Such a collection of translocation intermediates trapped in transition from the early to the late state of translocation reveals how elements of the mRNA-$tRNA_2$-growing peptide module are displaced over distances of approximately 30 to 50 Å and reach a close-to-final position of translocation. Moreover, the early translocation states presented hereinafter demonstrate how the eukaryotic translocase eEF2 engages spontaneously occurring, fully-rotated ribosomal conformations[21], while promoting peptidyl-tRNA translocation once it is fully accommodated on 80S. We describe the mechanism of maintenance of the eukaryotic translational reading frame on the atomic level, showing how eukaryote-specific elements of the 80S ribosome, eEF2 and tRNAs, undergo large-scale molecular rearrangements to safeguard the mRNA reading frame, from early eEF2 translocase accommodation, until the very late stages of the process.

Eukaryotic translocation intermediates

To visualize intermediates of the eukaryotic 80S ribosome translocation, we prepared translocating *S. cerevisiae* 80S ribosome complexes *in vitro*, using purified components, including naturally occurring *S. cerevisiae* eEF2. In the first set of experiments, complexes were prepared with the non-hydrolysable GTP analogue, GMPPCP, while in the second and third sets of experiments, the reaction mixture contained eEF2-binding translation inhibitor sordarin[22], and either GMPPCP or GTP (see Methods). All three reaction mixtures were subjected to single-particle cryo-EM analysis which yielded an ensemble of nine distinct reconstructions of *S. cerevisiae* 80S ribosome bound to the complete mRNA-$tRNA_2$ module (39-nucleotide mRNA, fMet-Phe-N-$tRNA^{Phe}$ and deacyl $tRNA^{fMet}$). Seven of these contained *S. cerevisiae* eEF2 bound to the ribosome, respectively representing genuine eukaryotic 80S ribosome translocation intermediates (TIs) (Fig. 1a, b, Extended Data Tables 1, 2, Supplementary Table 1). The tenth reconstruction resulted in a non-rotated (NR) state of *S. cerevisiae* 80S ribosome bound to mRNA, fMet-$tRNA^{fMet}$ and $tRNA^{fMet}$. Altogether, these structures reflect rotational motions of

the 40S small ribosomal subunit (SSU) from 0° to 11.7° relative to the 60S large subunit (LSU), SSU head-swiveling from 0° to 19.8°, as well as tRNA translocation trajectories accompanied by rearrangements of a number of intersubunit bridges and the L1 stalk (Fig. 1a-d, Extended Data Fig. 1, 2, Supplementary Fig. 1, 2a-d).

The most pronounced inter-subunit rotation of approximately 12° was observed in pre-translocation substrates, referred to as PRE-translocation-hybrid 1 (PRE-H1) and PRE-translocation-hybrid 2 (PRE-H2) complexes. These two early-stage complexes showed densities for peptidyl-tRNA in classical (A/A or A/A*), and deacyl-tRNA in hybrid P/E states (Fig. 1b, Supplementary Fig. 1). As such, the two states, determined at 1.97 Å and 2.72 Å, respectively, precede eEF2 recruitment on 80S and highlight a considerable shift of approximately 23 Å that the elbow of peptidyl-tRNA performs in its transition from A/A, in PRE-H1, to A/A*, in PRE-H2 (Supplementary Fig. 2b, c), confirming that tRNA acceptor arm movements can be uncoupled[7,23,24]. The NR complex (2.28 Å) has a non-swiveled head domain with tRNAs that occupy classical P/P and E/E states (Fig. 1a, b, Extended Data Fig. 1, Supplementary Fig. 1). Although no interactions between mRNA E-codon and $tRNA^{fMet}$ anticodon were found in NR, the latter displays final positions of tRNA translocation and thus reflects a POST-translocation state (POST).

Translocation intermediates 1 to 5 (TI-1 to TI-5) were determined in the presence of sordarin-bound native *S. cerevisiae* eEF2 (2.04-2.71 Å), while TI-1* and TI-4* complexes were reconstructed in the absence of the inhibitor (Fig 1a, b, Extended Data Tables 1, 2, Supplementary Table 1). TI-1, TI-1*, TI-3 and TI-4* were captured by GMPPCP, while TI-2, TI-4 and TI-5 were obtained from a single set of conditions in the presence of GTP and showed density for its hydrolyzed, GDP, form. Furthermore, we observed additional density in TI-4 corresponding to inorganic phosphate, Pi (Extended Data Fig. 3). The sequence of translocation events was reconstructed based on observed conformations of SSU domains (body and head rotation) and the exact positions of tRNAs and the L1 stalk (Extended Data Fig. 1, Supplementary Fig. 1, 2a-d, Supplementary Videos 1, 2,). Accordingly, TI-1 was defined as the earliest, while TI-5 represented the latest intermediate of eukaryotic translocation.

TI-1 and TI-1* are – to our knowledge – the first-ever visualized structures of an early eukaryotic ribosome translocation assembly, reflecting eEF2 recruitment events on 80S. Translocase

recruitment is accompanied by the opening of the SSU shoulder domain, while fMet-Phe-N-tRNA and deacyl $tRNA^{fMet}$ maintain A/A* and P/E configurations, respectively (Extended Data Fig. 1, Supplementary Fig. 1). Moreover, during early translocation events (PRE-H1, PRE-H2 and TI-1, TI-1*), the SSU head domain maintains a somewhat tilted position of approximately 1° relative to the body (Extended Data Fig. 1). Hence, the head domain likely acts as the main ligand anchor, modulating the progression of tRNA anticodons. Such importance of the head domain for tRNA translocation is further corroborated by a recent X-ray structure of an early intermediate state of eukaryotic translocation[3]. In this structure, eEF2 is fully accommodated, while the SSU body is still in a highly rotated state (9.5°), however, its SSU head domain has swiveled forward by 13°, coinciding with a major tRNA advancement.

During transitions from TI-2 to TI-5, 80S undergoes substantial large-scale conformational changes, where the SSU body domain rotates backward, being only 0.4° away (TI-5) from the final non-rotated position, while the SSU head domain performed forward rotation of up to 19.8° (Extended Data Fig. 1). Accommodation of eEF2 on 80S, as observed from TI-1 to TI-2 (Fig. 2a), coincides with further SSU shoulder domain opening. Then, as codon/anticodon duplexes undergo modest advancement from TI-2 to TI-5 (Fig. 1d), the mRNA-$tRNA_2$ module remains in the chimeric state (Extended Data Fig. 2, Supplementary Fig. 1). For instance, TI-2 and TI-3 states can be considered as "overlapping", however, even though GTP hydrolysis had already occurred in TI-2, TI-3 was considered more advanced since the SSU body is more back-rotated. Despite only a minor codon-anticodon advancement in late translocation, 80S undergoes substantial large-scale conformational changes in terms of SSU body back-rotation and SSU head forward swiveling (Extended Data Fig. 1).

Expectedly, the final product of translocation – in which eEF2 would have dissociated from the 80S ribosome complex, and fMet-Phe-N-$tRNA^{Phe}$ and deacyl-$tRNA^{fMet}$ reached P/P and E/E positions, respectively – was not observed in any of the assayed *in vitro* conditions. This confirms that the translocation process cannot be fully accomplished in the absence of GTP hydrolysis[25] or in the presence of sordarin[22]. Thus, our study supports the proposal that the elongating complex can reach a close-to-final state in a single round of translocation with no requirements for energy coming directly from GTP hydrolysis[26]. Analogously, final translocation events, including notably eEF2 dissociation, would therefore require the hydrolyzed, GDP, form[25]. Ultimately, the

translocase is most likely to guard against the slippage of the translational reading frame, while the principal role of GTP hydrolysis is to ensure eEF2 will not be released from the ribosome before completion of the translocation cycle[4,25,27].

eEF2 engagement and mRNA-tRNA$_2$ movement

Early translocation intermediates TI-1 and TI-1* reveal eEF2 binding to a fully rotated hybrid intermediate ribosome captured in a conformation analogous to PRE-H2 (Fig. 1a, b, Supplementary Fig. 1). Displacement of the elbow domain of peptidyl-tRNA, which prevents the collision with domain IV of eEF2 (Fig. 2b), as well as the movement of the acceptor stem of deacyl-tRNA from P/P to P/E, demonstrate that PRE-H2 represents an authentic translocation intermediate, in which acceptor stems of tRNAs had largely translocated on the LSU. This step occurs spontaneously, in the absence of both eEF2 and GTP, and can be reversible[28]. The TI-1 state is captured during eEF2 recruitment on 80S, with domains I and V bound to the universally conserved sarcin-ricin loop (SRL) of 25S rRNA (Fig. 2c, Extended Data Fig. 4a-d). Moreover, domain I is accommodated on uL6, domain V is in contact with uL11, while domain IV is found between SSU shoulder and head domains. The TI-1 structure also reveals eukaryote-specific points of contact between eEF2 domains I and II and SSU proteins eS6 and eS24 (Extended Data Fig. 4e). In addition, the lysine-rich loop 1 of domain IV forms initial contacts with the peptidyl-tRNA anticodon-stem loop (ASL), notably through a hydrogen bond with proline residue 580 (Fig. 2d, e). Although the interaction is not side-chain-specific, it points to the fundamental importance of proline geometry for domain IV conformation in the context of translocation accuracy. Indeed, single-point mutation of proline 580 to histidine increases the rate of frameshifting events in yeast, while the equivalent P596H in human eEF2 is associated with human neurodegeneration phenotypes, notably autosomal dominant spinocerebellar ataxias[29].

During progression to TI-2, eEF2 undergoes rotation-like movement by approximately 17° around SRL, and ultimately, accommodates on 80S (Fig. 2c). In the transition from TI-1 to TI-2, unlocking of the decoding center enables eEF2 domain IV to move into the A-site by approximately 19 Å and engage in direct interactions with the minor groove of the codon-anticodon duplex formed by peptidyl-tRNA and the A-codon (Fig. 2f, Fig. 3a, b, Supplementary Video 3). Full accommodation of eEF2 occurs together with further SSU back rotation (Fig. 1a-b,

2a, c, Extended Data Fig. 1). These observations further suggest that unlocking of the eukaryotic ribosome decoding center occurs during the transition from TI-1 to the early translocation state characterized by the recent crystal structure of eukaryotic *S. cerevisiae* 80S ribosome[3]. Disruption of minor groove interactions between rRNA elements of the decoding center and the codon-anticodon duplex in the SSU A-site presents a rate-limiting step in enzymatic translocation[30]. Upon sequential transitions from TI-2 to TI-5, accompanied by further reverse rotation of the SSU body and forward swiveling of the head, the mRNA-$tRNA_2$ cargo reaches its close-to-final position of translocation, while eEF2 domain IV conserves its overall conformation and position on the SSU (Extended Data Fig. 2, 5a-c, Supplementary Fig. 1). Furthermore, structures of TI-1 and TI-3 obtained in the presence of GMPPCP showed that abrogation of GTP hydrolysis does not prevent translocation from reaching a late intermediate state (Extended Data Fig 2, 3, Supplementary Fig. 1). Therefore, eEF2 contributes to translocation most likely by preventing reverse rotation of the SSU head domain, acting as a molecular "doorstop"[3,4] (Supplementary Video 4).

Although we observed gradual dissociation of eEF2 from 80S during transitions from TI-2 to TI-5 (Extended Data Fig. 4b-d), contacts between eEF2 domain IV and peptidyl-tRNA are maintained (Fig. 2d-f, Extended data Fig. 5b). More importantly, eEF2 contributes substantially to the overall stability of the mRNA-$tRNA_2$ module, with an additional contact area of ~430 $Å^2$ in TI-2, TI-3 and TI-4. As such, it accounts for roughly 25 % of the total contact area found to preserve the integrity of codon-anticodon duplexes, including tRNA ASLs. Our data suggest that codon-anticodon integrity is maintained until the very late stages of the translocation process, pointing to the possible existence of accuracy control mechanisms, not only upon decoding but throughout the elongation cycle.

mRNA reading frame and eEF2 domain IV

Our high-resolution structures reveal an intricate network of interactions preventing the slippage of the translational reading frame (Fig. 3a). First, as eEF2 is recruited on the hybrid 80S complex and TI-1 is formed, the codon-anticodon duplex of peptidyl-tRNA remains locked in the decoding center – as observed in PRE-H1/PRE-H2 – while the stem of peptidyl-tRNA ASL gains additional stability from domain IV of not fully accommodated eEF2 (Fig. 2d-e). In the decoding

center, the codon-anticodon duplex is secured by a highly ordered network of interactions, largely resembling the one previously described in prokaryotes[31]. However, we observed additional interactions with the eukaryote-specific glutamine residue 63 of the conserved uS12 protein (Fig. 3a). Then, upon transition from TI-1 to TI-2 and full eEF2 accommodation, the tRNA-like domain IV of eEF2 establishes an intensive network of interactions with the codon-anticodon duplex, in which diphthamide forms a total of three hydrogen bonds with the second base pair (BP2), involving both codon and anticodon nucleotides (Fig. 3a, b). A similar pattern of interactions, although with additional interactions with BP1, was recently described in a TI trapped presumably at a state between TI-1 and TI-2[3]. Next, reconstructions of TI-3 and TI-4 suggest that the interaction network of diphthamide undergoes remodeling to include an additional contact with the third codon nucleotide, possibly by means of amide O-protonation. Finally, in TI-5, diphthamide re-establishes the interaction network only with the second codon nucleotide. This suggests that diphthamide acts by maintaining the interaction with BP2 throughout translocation, while transiently probing BP1 during early[3], and BP3 during late translocation. Stabilization of the codon-anticodon duplex is further ensured by histidine 583 of eEF2 domain IV, found to interact with the phosphate moiety of wybutosine 37 of $tRNA^{Phe}$ (Fig. 2f) from the early[3] to the late state of almost accomplished translocation (TI-5). In addition to the stabilizing effect of eEF2, the codon-anticodon duplex is also secured by RNA nucleotides of the SSU body domain (Fig.3a) Our cryo-EM data also show that BP2 gains additional stabilization in TI-3 onwards through an additional hydrogen bond with the ribosomal residue U1761. Moreover, wobble base pair geometry in TI-4 and TI-5 is further secured by a hydrogen bond with Cm1639, which complements BP3 interacting counterparts C1637, G1638 and C1640 preserved from TI-2. Altogether, these interactions mimic the stabilizing effect of the decoding center observed in TI-1. Ultimately, the sterically constrained environment imposed predominantly on BP2 through the arrangement of diphthamide and domain IV residues suggests that the role of eEF2 is not only to stabilize correct Watson-Crick codon-anticodon interactions but also to contribute to tRNA discrimination during translocation (Fig. 3c). By probing the minor groove of the peptidyl-tRNA codon-anticodon duplex, eEF2 could uncover near-cognate peptidyl-tRNA paired to the codon by non-canonical Watson-Crick interactions and trigger dissociation of erroneous peptidyl-tRNA from the eukaryotic ribosome[32].

Ribosome mRNA-tRNA interactions

The most expanded interaction networks between mRNA and the eukaryotic elongating ribosome were observed in hybrid and TI-1 states (e.g. PRE-H1 in Extended Data Fig. 6a, b), when A-tRNA binding to the NR complex led to the narrowing of the downstream mRNA tunnel, as shown in the bacterial ribosome[33], while the SSU head domain remained unrotated. mRNA is found to interact with uS12 and a number of 18S nucleotides in a base-non-specific manner (Extended Data Fig. 6c). All interacting elements are conserved from prokaryotes, except the eukaryote-specific Gln63 of uS12. The transition from TI-1 to subsequent late TIs leads to simultaneous disruption of the pre-translocation arrangement and formation of new post-translocation interactions of peptidyl- and deacyl-tRNA ASLs with the SSU body domain (Fig. 4a-d). Unlike deacyl-tRNA, peptidyl-tRNA ASL interacts primarily with the SSU body rather than the head domain. This principally arises from the interactions with decoding nucleotides in TI-1 (Fig. 3a) and hybrid states. During late translocation (from TI-2 to TI-5), a preserved set of SSU body nucleotides ensures both the advancement of peptidyl-tRNA ASL through chimeric states (e.g. TI-4 in Fig. 4c) and the final delivery to the classical state in NR, while deacyl-tRNA is almost exclusively "guided" by the SSU head domain (Fig. 4c, d). Ultimately – as deacyl-tRNA reaches the classical E-site – SSU head domain residues disengage from its ASL as a result of head domain back-swiveling to the classical NR state, and restore the complete P-site setup around peptidyl-tRNA (Fig. 4d). Subsequent disruption of these interactions may be the main energy barrier to the rate-limiting step of unlocking, which is to be solved by eEF2. Indeed, following the unlocking event, eEF2 domain IV mimics the effect of decoding nucleotides to maintain the stability of weak A-codon-anticodon pairing of peptidyl-tRNA and prevent the loss of the reading frame during translocation (Fig. 3a, 4a-d).

Eukaryote-specific RNA modifications

1-methyl-3-α-amino-α-carboxyl-propyl pseudouridine 1191 ($m^1acp^3\Psi1191$) is the only hypermodification identified in *S. cerevisiae* rRNA. This heavily modified uridine[34], reported in the hairpin loop of the universally conserved helix 31 of 18S rRNA, lies at the interface of SSU head and body domains, and is known to participate in the architecture of the peptidyl-tRNA site[35,36] (Fig. 5a). The central importance of $m^1acp^3\Psi1191$ is underlined by the fact that its loss

(hypo-modification) is associated with the proliferation of colorectal cancer cells[37]. In the classical (NR) state, this hypermodification interacts with the first anticodon nucleotide of the P-site tRNA, while forming a hydrogen bond with C1637 of the SSU body. This SSU head-to-body contact at positions 1191-1637 is then maintained during the transition to the rotated state (Fig. 5a). Despite its subsequent disruption due to eEF2 binding and forward head swiveling-associated translocation of P-site tRNA, $m^1acp^3\Psi$1191 maintains the interaction with tRNA and guides the ASL to the E-site while covering a distance of approximately 11 Å. Finally, as deacyl-tRNA reaches its final position and the head swivels backward, $m^1acp^3\Psi$1191 releases E-site tRNA and immediately reaches to the next P-site tRNA ready to engage in the upcoming step of translocation (Fig. 5a, Supplementary Video 5).

Our structures also revealed additional stabilization of codon-anticodon pairing in which the wyosine moiety of the hypermodified wybutosine 37 of *S. cerevisiae* $tRNA^{Phe}$ (yW37) cross-strand stacks with the first codon nucleoside paired to peptidyl-$tRNA^{Phe}$ (Fig. 5b). As translocation reaches the late states, tighter compactness of the peptidyl-tRNA ASL can be observed. Wybutosine modulates this compactness by protruding further into the interior of the ASL and directly interacting with U32, which decreases the conformational flexibility of the anticodon loop[38]. Overall, these findings substantiate previous studies which showed that both the absence of yW37 and its alterations increased the ribosomal frameshifting frequency[39] while being linked to a lower survival of patients with cancer[40].

Sordarin action and eEF2 dissociation

Reconstructions of TI-1, TI-2, TI-3, TI-4 and TI-5 revealed additional density at the interface of eEF2 domains III and V corresponding to sordarin[41] (Extended Data Fig. 7a-j). Global alignments of ribosome-bound eEF2 in early and late states of translocation suggest that the presence of sordarin has insignificant effects on the overall conformation of eEF2[5] and, more importantly, has little-to-no effect neither on the position nor the conformation of eEF2 domains I and IV relative to the 80S ribosome (Extended Data Fig. 7a-c). However, eEF2 domain III alignment indicates that sordarin bridges the domain III-V interface (Extended Data Fig. 7d-i). Consequently, the mechanism of sordarin-induced eEF2 stalling on the 80S ribosome most likely proceeds by domain interface remodeling. Late translocation (TI-2 to TI-5) is associated with a

stepwise decrease of the overall contact area between eEF2 and, both the full 80S, and the individual subunits (Extended Data Fig. 4b-d), however, the interactions of eEF2 domain II with the SSU shoulder protein uS12 expand as the entire SSU body domain rotates backward (Extended Data Figs. 1, 8a, b). Structural analyses corroborate these findings and reveal that uS12 prevents further progression of eEF2 on the SSU (Extended Data Fig. 8a). The interactions between eEF2 domain III and uS12 follow the overall decreasing trend of eEF2/80S contacts only until the penultimate translocation state TI-4, from where the contact area between domain III and uS12 increases (Extended Data Fig. 4b-d, 8b). Indeed, our structures reveal that the α-helix A of domain III swings in the direction of domain V, which in turn can trigger eEF2 dissociation from the translocating ribosomal assembly, as proposed in earlier works on non-canonical IRES-mediated translocation[42]. Recently, Carbone *et al*. observed a similar trend in EF-G domain III rearrangement relative to uS12 in a late bacterial translocation state where EF-G dissociation had already commenced and the GTPase domain had unbound from the ribosome[7]. We propose that the mechanism of sordarin action most likely consists in blocking the full remodeling of eEF2 domain III with respect to domain V, which possibly leads to eEF2 stalling on 80S, and ultimately, late translocation arrest. We cannot exclude that sordarin action on eEF2 might inhibit conformational changes of the switch loop 2 (sw2) through a similar mechanism proposed for argyrin B (ArgB)[43] (Extended Data Fig. 7g-i). As for ArgB, sordarin seems to indirectly prevent sw2 remodeling, which is expected to be necessary for eEF2 dissociation. In comparison, fusidic acid (FA), a bacterial EF-G-targeting antibiotic, binds to a distinct site vacated by the released inorganic phosphate and – unlike sordarin and ArgB – blocks eEF2 by directly stabilizing the GTP-like conformation of sw2[6]. However, in contrast to FA and ArgB, which trap the mid-translocation intermediate INT2[6,43], sordarin allows the eukaryotic translocating assembly to reach the late intermediate state TI-5. Finally, our TI-4 showed density for inorganic phosphate, suggesting that in the presence of sordarin, and without phosphate release or domain IV remodeling, translocation is almost fully accomplished, and a late chimeric state can be formed.

Discussion

Here we present first atomic-resolution structural information for the understanding of the mechanism of movement of the mRNA-$tRNA_2$-growing peptide module during protein synthesis in eukaryotes. We characterize eukaryotic translocation intermediates whose existence had only been hypothesized on the basis of bacterial translocation but their reconstructions had never been reported. Our data describe how the eukaryotic translocase eEF2 is engaged by a spontaneously rotated 80S ribosome and reveal the importance of its contacts with co-evolved eukaryote-specific SSU proteins. This study reveals that the additional complexity of the eukaryotic translational apparatus, in comparison with the prokaryotic system, reflects more sophisticated and more finely regulated mechanisms of maintenance of the mRNA-$tRNA_2$ module during its translocation through the ribosome. An extensive system of eukaryote-specific rRNA and tRNA post-transcriptional modifications, together with eEF2 and its unique post-translational modification, actively contribute to the accuracy of protein synthesis by preventing the slippage of the translational reading frame (Supplementary Video 6).

We propose that the sterically constrained environment imposed by the eukaryote-specific post-translational modification diphthamide, in the context of domain IV conformation, not only stabilizes correct Watson-Crick codon-anticodon interactions but may uncover the erroneous peptidyl-tRNA by probing the minor groove of the codon-anticodon duplex. Therefore, this additional proofreading mechanism that prevents incorporation of an incorrect amino acid during translocation contributes to higher accuracy of protein synthesis in eukaryotes. Our reconstructions in the presence of GMPPCP demonstrated nearly complete movement of the $tRNA_2$-mRNA module, corroborating the model in which the translocase functions as a molecular "doorstop" which uncouples the mRNA-$tRNA_2$ movement from the thermally driven back-rotation of the SSU body/platform[23,26,27,42,44,45]. Hence, it seems that the primary role of GTP hydrolysis in translocation in all kingdoms of life is to establish an irreversible step that prevents translocase release until both tRNAs and mRNA have moved by one full codon. Such a mechanism would ensure productive translocation and efficient maintenance of the translational reading frame[3,6,7,25].

Here we propose the mechanism of translocation inhibition by sordarin. The latter can bind to ribosome-associated eEF2 from the early TI-1 state and seems not to affect global eEF2 conformation or otherwise interfere with subsequent eEF2 accommodation on the ribosome. As

translocation then reaches the late TI-5 state, sordarin supposedly stalls eEF2 on the ribosome by preventing domain III remodeling and ultimate dissociation from the ribosome.

Although our results provide atomic resolution information on molecular mechanisms of eukaryotic ribosome translocation, further structural studies, including time-resolved cryo-EM and biochemical investigations of mRNA-tRNA displacement through the eukaryotic ribosome, are needed to provide full understanding of the precise timing of GTP hydrolysis and Pi release, as well as translocation proofreading mechanisms that ensure accurate protein synthesis in eukaryotes.

References

1 Ortiz, P. A., Ulloque, R., Kihara, G. K., Zheng, H. & Kinzy, T. G. Translation elongation factor 2 anticodon mimicry domain mutants affect fidelity and diphtheria toxin resistance. *J. Biol. Chem.* **281**, 32639-32648 (2006).

2 Liu, S. *et al.* Diphthamide modification on eukaryotic elongation factor 2 is needed to assure fidelity of mRNA translation and mouse development. *Proc. Natl. Acad. Sci. U. S. A.* **109**, 13817-13822 (2012).

3 Djumagulov, M. *et al.* Accuracy mechanism of eukaryotic ribosome translocation. *Nature* **600**, 543-546 (2021).

4 Flis, J. *et al.* tRNA Translocation by the Eukaryotic 80S Ribosome and the Impact of GTP Hydrolysis. *Cell Rep* **25**, 2676-2688 e2677 (2018).

5 Taylor, D. J. *et al.* Structures of modified eEF2 80S ribosome complexes reveal the role of GTP hydrolysis in translocation. *EMBO J.* **26**, 2421-2431 (2007).

6 Rundlet, E. J. *et al.* Structural basis of early translocation events on the ribosome. *Nature* **595**, 741-745 (2021).

7 Carbone, C. E. *et al.* Time-resolved cryo-EM visualizes ribosomal translocation with EF-G and GTP. *Nat Commun* **12**, 7236 (2021).

8 Petrychenko, V. *et al.* Structural mechanism of GTPase-powered ribosome-tRNA movement. *Nat Commun* **12**, 5933 (2021).

9 Zhou, J., Lancaster, L., Donohue, J. P. & Noller, H. F. How the ribosome hands the A-site tRNA to the P site during EF-G-catalyzed translocation. *Science* **345**, 1188-1191 (2014).

10 Zhou, J., Lancaster, L., Donohue, J. P. & Noller, H. F. Crystal structures of EF-G-ribosome complexes trapped in intermediate states of translocation. *Science* **340**, 1236086 (2013).

11 Ramrath, D. J. *et al.* Visualization of two transfer RNAs trapped in transit during elongation factor G-mediated translocation. *Proc. Natl. Acad. Sci. U. S. A.* **110**, 20964-20969 (2013).

12 Melnikov, S. *et al.* One core, two shells: bacterial and eukaryotic ribosomes. *Nat. Struct. Mol. Biol.* **19**, 560-567 (2012).

13 Budkevich, T. V. *et al.* Regulation of the mammalian elongation cycle by subunit rolling: a eukaryotic-specific ribosome rearrangement. *Cell* **158**, 121-131 (2014).

14 Dever, T. E., Dinman, J. D. & Green, R. Translation Elongation and Recoding in Eukaryotes. *Cold Spring Harb. Perspect. Biol.* **10** (2018).

15 Iglewski, B. H. & Kabat, D. NAD-dependent inhibition of protein synthesis by Pseudomonas aeruginosa toxin. *Proc. Natl. Acad. Sci. U. S. A.* **72**, 2284-2288 (1975).

16 Lee, H. & Iglewski, W. J. Cellular ADP-ribosyltransferase with the same mechanism of action as diphtheria toxin and Pseudomonas toxin A. *Proc. Natl. Acad. Sci. U. S. A.* **81**, 2703-2707 (1984).

17 Arguelles, S., Camandola, S., Cutler, R. G., Ayala, A. & Mattson, M. P. Elongation factor 2 diphthamide is critical for translation of two IRES-dependent protein targets, XIAP and FGF2, under oxidative stress conditions. *Free Radic. Biol. Med.* **67**, 131-138 (2014).

18 Hawer, H. *et al.* Diphthamide-deficiency syndrome: a novel human developmental disorder and ribosomopathy. *Eur. J. Hum. Genet.* **28**, 1497-1508 (2020).

19 Shankar, S. P. *et al.* A novel DPH5-related diphthamide-deficiency syndrome causing embryonic lethality or profound neurodevelopmental disorder. *Genet. Med.* **24**, 1567-1582 (2022).

20 Stahl, S. *et al.* Loss of diphthamide pre-activates NF-kappaB and death receptor pathways and renders MCF7 cells hypersensitive to tumor necrosis factor. *Proc. Natl. Acad. Sci. U. S. A.* **112**, 10732-10737 (2015).

21 Chen, J., Tsai, A., O'Leary, S. E., Petrov, A. & Puglisi, J. D. Unraveling the dynamics of ribosome translocation. *Curr. Opin. Struct. Biol.* **22**, 804-814 (2012).

22 Justice, M. C. *et al.* Elongation factor 2 as a novel target for selective inhibition of fungal protein synthesis. *J. Biol. Chem.* **273**, 3148-3151 (1998).

23 Munro, J. B., Altman, R. B., O'Connor, N. & Blanchard, S. C. Identification of two distinct hybrid state intermediates on the ribosome. *Mol. Cell* **25**, 505-517 (2007).

24 Budkevich, T. *et al.* Structure and dynamics of the mammalian ribosomal pretranslocation complex. *Mol. Cell* **44**, 214-224 (2011).

25 Rexroad, G., Donohue, J. P., Lancaster, L. & Noller, H. F. The role of GTP hydrolysis by EF-G in ribosomal translocation. *Proc. Natl. Acad. Sci. U. S. A.* **119**, e2212502119 (2022).

26 Inoue-Yokosawa, N., Ishikawa, C. & Kaziro, Y. The role of guanosine triphosphate in translocation reaction catalyzed by elongation factor G. *J. Biol. Chem.* **249**, 4321-4323 (1974).

27 Kaziro, Y. The role of guanosine 5'-triphosphate in polypeptide chain elongation. *Biochim. Biophys. Acta* **505**, 95-127 (1978).

28 Cornish, P. V., Ermolenko, D. N., Noller, H. F. & Ha, T. Spontaneous intersubunit rotation in single ribosomes. *Mol. Cell* **30**, 578-588 (2008).

29 Hekman, K. E. *et al.* A conserved eEF2 coding variant in SCA26 leads to loss of translational fidelity and increased susceptibility to proteostatic insult. *Hum. Mol. Genet.* **21**, 5472-5483 (2012).

30 Khade, P. K. & Joseph, S. Messenger RNA interactions in the decoding center control the rate of translocation. *Nat. Struct. Mol. Biol.* **18**, 1300-1302 (2011).

31 Demeshkina, N., Jenner, L., Westhof, E., Yusupov, M. & Yusupova, G. A new understanding of the decoding principle on the ribosome. *Nature* **484**, 256-259 (2012).

32 Zaher, H. S. & Green, R. Fidelity at the molecular level: lessons from protein synthesis. *Cell* **136**, 746-762 (2009).

33 Jenner, L. B., Demeshkina, N., Yusupova, G. & Yusupov, M. Structural aspects of messenger RNA reading frame maintenance by the ribosome. *Nat. Struct. Mol. Biol.* **17**, 555-560 (2010).

34 Meyer, B. *et al.* The Bowen-Conradi syndrome protein Nep1 (Emg1) has a dual role in eukaryotic ribosome biogenesis, as an essential assembly factor and in the methylation of Psi1191 in yeast 18S rRNA. *Nucleic Acids Res.* **39**, 1526-1537 (2011).

35 Ben-Shem, A. *et al.* The structure of the eukaryotic ribosome at 3.0 A resolution. *Science* **334**, 1524-1529 (2011).

36 Ben-Shem, A., Jenner, L., Yusupova, G. & Yusupov, M. Crystal Structure of the Eukaryotic Ribosome. *Science* **330**, 1203-1209 (2010).

37 Babaian, A. *et al.* Loss of m(1)acp(3)Psi Ribosomal RNA Modification Is a Major Feature of Cancer. *Cell Rep* **31**, 107611 (2020).

38 Stuart, J. W., Koshlap, K. M., Guenther, R. & Agris, P. F. Naturally-occurring modification restricts the anticodon domain conformational space of tRNA(Phe). *J. Mol. Biol.* **334**, 901-918 (2003).

39 Carlson, B. A. *et al.* Transfer RNA modification status influences retroviral ribosomal frameshifting. *Virology* **255**, 2-8 (1999).

40 Rossello-Tortella, M. *et al.* Epigenetic loss of the transfer RNA-modifying enzyme TYW2 induces ribosome frameshifts in colon cancer. *Proc. Natl. Acad. Sci. U. S. A.* **117**, 20785-20793 (2020).

41 Jorgensen, R. *et al.* Two crystal structures demonstrate large conformational changes in the eukaryotic ribosomal translocase. *Nat. Struct. Biol.* **10**, 379-385 (2003).

42 Murray, J. *et al.* Structural characterization of ribosome recruitment and translocation by type IV IRES. *Elife* **5** (2016).

43 Wieland, M. *et al.* The cyclic octapeptide antibiotic argyrin B inhibits translation by trapping EF-G on the ribosome during translocation. *Proc. Natl. Acad. Sci. U. S. A.* **119**, e2114214119 (2022).

44 Pestka, S. Studies on the formation of transfer ribonucleic acid-ribosome complexes. 3. The formation of peptide bonds by ribosomes in the absence of supernatant enzymes. *J. Biol. Chem.* **243**, 2810-2820 (1968).

45 Yusupova, G. Z., Belitsina, N. V. & Spirin, A. S. Template-free ribosomal synthesis of polypeptides from aminoacyl-tRNA. Polyphenylalanine synthesis from phenylalanyl-tRNALys. *FEBS Lett.* **206**, 142-146 (1986).

Methods

Purification of *S. cerevisiae* 80S ribosome

S. cerevisiae 80S ribosomes were purified from the JD1370-ΔStm1 strain[46] following a previously published protocol with minor modifications[35]. After cell disruption, ribosomes were isolated by PEG 20,000 precipitation between 4 % and 8.5 % w/v and purified on 15-30 % w/v sucrose gradients (20 mM HEPES/KOH pH 7.5, 120 mM KCl, 10 mM $MgCl_2$, 10 % w/v sucrose, 2 mM DTT, 0.37 mM EDTA, 2.5 mM spermidine). The peak of 80S ribosomes was pooled, precipitated by PEG 20,000 and subsequently re-dissolved in buffer G (10 mM HEPES/KOH pH 7.5, 50 mM CH_3COOK, 10 mM NH_4Cl, 5 mM $(CH_3COO)_2Mg$, 2 mM DTT).

Purification of endogenous *S. cerevisiae* eEF2

Native eEF2 was isolated from the *S. cerevisiae* JD1370-ΔStm1 strain according to a previously reported protocol[47] with some modifications. Following microfluidizer cell disruption and lysate dialysis, eEF2 was purified on HiLoad® SP Sepharose® and Q Sepharose®, after which the sample was applied to a HiLoad® 16/600 Superdex® 200 pg gel filtration column (all from GE Healthcare). Eluted eEF2 fractions were concentrated and stored in 20 mM HEPES/KOH pH 7.5, 10 % v/v glycerol, 5 mM $MgCl_2$, 1 mM DTT, 100 mM KCl.

Purification and aminoacylation of tRNAs

Amino-tailing of *S. cerevisiae* $tRNA^{Phe}$ (replacement of the 3'-terminal A76 nucleotide carrying the 3'-OH group with the one carrying 3'-NH_2) was performed as previously reported[48] with some modifications. A mixture containing 40 µM deacylated native *S. cerevisiae* $tRNA^{Phe}$ (Sigma-Aldrich), 1 mM 3'-amino-3'-deoxyadenosine-5'-O-triphosphate (Biolog Life Science Institute GmbH), 1 mM sodium pyrophosphate (Sigma-Aldrich), 70 µM CCA-adding enzyme, 10 mM $MgCl_2$, 100 mM glycine/NaOH pH 9, 1 mM DTT was incubated at 37°C for one hour and 20 minutes. The reaction was terminated by addition of EDTA to 20 mM, treated with 1:1 phenol-chloroform mixture and precipitated with ethanol. The pellet was washed two times, dissolved in 30 µL of 10 mM Hepes/KOH pH 7.5 and purified on a Sephadex® G-25 spin column (Sigma-Aldrich). The resulting, full-length, *S. cerevisiae* 3'-NH_2-$tRNA^{Phe}$ was enzymatically acylated with phenylalanine as previously described[49] with minor modifications.

S. cerevisiae Phe-N-tRNA^{Phe} was purified on a Waters™ C4 column (Delta-Pak C4, 300Å, 5 µm, 3.9 mm X 150 mm, 1K - 30K, 1/pk) by applying a linear ethanol gradient (as reported in [50]) and stored in 20 mM CH_3COONH_4 pH 5.
Following purification of its overexpressed form, *E. coli* initiator tRNA^{fMet} was aminoacylated and formylated according to previously published protocols[51]. The reaction mix was phenol-extracted and the aqueous phase was applied to a TSKgel® Phenyl-5PW column (Tosoh bioscience). Purified fractions of fMet-tRNA^{fMet} were stored in 20 mM CH_3COONH_4 pH 5.

Formation of 80S ribosome translocation complexes

For reconstitution of translocation complexes 80S/tRNA$_2$/mRNA/eEF2/GMPPCP or 80S/tRNA$_2$/mRNA/eEF2/GTP, *S. cerevisiae* 80S ribosomes (2.2 µM) and 39 nucleotide-long mRNA (5'-AAAAGAAAAGAAAAGAAAAUGUUUUUUGAAGAAAAGAAA-3', Dharmacon) (10.8 µM) were incubated at 30°C for 10 minutes in 10 mM HEPES/KOH pH 7.5, 50 mM CH_3COOK, 10 mM NH_4Cl, 5 mM $(CH_3COO)_2Mg$, 2 mM DTT. *E. coli* fMet-tRNA^{fMet} (10.8 µM) and *S. cerevisiae* Phe-N-tRNA^{Phe} (10.8 µM) were then added in two steps and incubation continued for 5 and 3 minutes, respectively. Separately, *S. cerevisiae* eEF2 (10.8 µM) was incubated either with GMPPCP (255 µM) or GTP (255 µM) for 10 minutes at room temperature. Each of the two eEF2 mixtures was then added to the ribosome mix and buffer conditions were re-adjusted to 10 mM HEPES/KOH pH 7.5, 50 mM CH_3COOK, 10 mM NH_4Cl, 6 mM $(CH_3COO)_2Mg$ and 1.25 mM DTT. Additionally, if present, sordarin (Sigma-Aldrich) was added at this stage to a final concentration of 100 µM. The last incubation step proceeded for another 10 minutes at 30°C.

Cryo-EM grid preparation and data collection

Following complex formation, 3 µL of sample were applied to glow-discharged Ultrathin Carbon Quantifoil® R 2/2 on 300 gold mesh (Jena Bioscience) using a Mark IV Vitrobot™ (Thermo Fisher Scientific). Incubation of grids at 9°C and 95% humidity lasted for 30 seconds and was immediately followed by blotting and flash freezing in liquid ethane, pre-cooled to the liquid nitrogen temperature. Grid screening was performed on a 200 kV Glacios transmission electron

microscope (Thermo Fisher Scientific) equipped with a K2 Summit direct electron detector (Gatan).

Single molecule datasets were acquired at the Dubochet Center for Imaging of EPFL and the University of Lausanne (DCI-Lausanne) on a 300 kV Titan Krios G4i transmission electron microscope (Thermo Fisher Scientific) equipped with a Cold FEG emission gun, SelectrisX energy filter and a Falcon IV direct electron detector. Datasets were collected using the EPU automated software (Thermo Fisher Scientific) and a pixel size at detector of 0.450 Å/pix (for eEF2/GMPPCP and eEF2/GTP datasets with sordardin) and 0.726 Å/pix (for the eEF2/GMPPCP dataset without sordarin). Total electron exposure was set to 60 e^- per $Å^2$ for the eEF2/GTP/sordarin dataset and 40 e^- per $Å^2$ for both eEF2/GMPPCP and eEF2/GMPPCP/sordarin datasets.

Cryo-EM data processing of the 80S/eEF2/GTP/sordarin elongation complex

Cryo-EM image processing was performed using cryoSPARC[52]. Raw micrographs were motion-corrected, and CTF estimation was carried out. A total of 616,978 particles were auto-picked and extracted with fourier cropping 4 times (bin4 data). Several rounds of 2D classification were performed, and an ab initio structure was reconstructed and used for initial 3D variability analysis[53]. The resulting volumes were subjected to heterogeneous refinement against a total of 442,508 particles from selected 2D classes. This resulted in four structures, each representing different rotational states of the 40S subunit. Three meaningful classes were selected and subjected to additional 3D variability analysis, resulting in three subclasses for each class.

The first class consisted of 170,386 particles with the fully rotated 40S subunit. Its first subclass contained both deacyl- and peptidyl-tRNAs, but no eEF2. This sub-population was re-extracted (bin2), and homogeneous refinement yielded the PRE-H1 complex (55,455 particles). Although two other subclasses contained the elongation factor and were refined to high resolution, they were not further examined due to the absence of peptidyl-tRNA.

The second class of 133,186 particles with a semi-rotated 40S subunit resulted in subclasses, all of which contained deacyl- and peptidyl-tRNAs and eEF2. Particle re-extraction (bin2), followed by respective homogeneous refinements, resulted in two intermediate translocation structures, TI-2 (58,531 particles) and TI-4 (55,762 particles).

Finally, the third class with 133,186 particles and a non-rotated 40S subunit also yielded three subclasses. The first subclass possessing only tRNAs was pooled and local refinement yielded the NR complex (21,458 particles). Two remaining subclasses contained clear density for eEF2. The meaningful class (51,517 particles) was subjected to additional 3D variability analysis and a well resolved sub-population was re-extracted (bin2) and processed by homogenous refinement which yielded the TI-5 complex (23,773 particles).

Cryo-EM data processing of the 80S/eEF2/GMPPCP/sordarin elongation complex

Raw micrographs were motion corrected and CTF estimated[52]. 514,460 particles were auto-picked and extracted with fourier cropping 4 times (bin4). Two rounds of 2D classification were performed, good 2D classes were selected and 393,786 particles were re-extracted. Consensus homogenous refinement was performed, and the volume was applied to 3D variability analysis[53]. The class with the rotated 40S subunit (42,053 particles) was subjected to 3D variability analysis which resulted in four subclasses. Only the subclasses possessing density for both tRNAs and eEF2 were selected, particles were re-extracted (bin2) and homogenous refinement yielded the TI-1 complex (23,096 particles).
Classes with the semi-rotated 40S subunit were combined and run through 3D variability analysis yielding five subclasses. Three of the five subclasses showed strong density for both tRNAs and eEF2. They were pooled together, particles were re-extracted (bin2) and refined, yielding the TI-3 complex (73,086 particles).

Cryo-EM data processing of the 80S/eEF2/GMPPCP elongation complex

Raw micrographs were motion corrected, CTF estimated, particles were auto-picked and extracted with fourier cropping 4 times (bin4). Selected 2D classes yielding 561,498 particles were used to refine the initial volume. Next, particles were subjected to 3D variability analysis and separated either on the basis of 40S subunit rotation (workflow 1) or presence of strong density of tRNA and eEF2 ligands (workflow 2).
In workflow 1, the population containing rotated 40S (157,099 particles) was re-extracted (twofold binned) and subject to a new round of 3D variability analysis. One of the resulting subclasses contained deacyl- and peptidyl-tRNAs, but no elongation factor 2. Particles were re-

extracted without fourier cropping (fully un-binned, bin1) and supplied to homogenous refinement which yielded the PRE-H2 structure (68,945 particles). The second subclass with the non-rotated 40S (118,986 particles) was re-extracted and subjected to 3D variability analysis, and only the sub-population with strong tRNA density was pooled. Particles were then re-extracted (bin2) and applied to homogenous refinement which yielded the TI-4* complex (41,878 particles).
In workflow 2, 276,089 particles possessing strong tRNA and eEF2 density were selected from initial 3D variability analysis. Following, two series of additional 3D variability analysis, only particles with strong ligand density were pooled. This sub-population was re-extracted (bin2) and supplied to homogenous refinement which yielded the TI-1* complex (22,551 particles).

Model building and refinement

PDB ID 7OSM was split into 60S, 40S body and head domains, eEF2 and deacyl-tRNA. Sub-models were then rigid fitted into cryo-EM maps using the *fitmap* command in ChimeraX[54,55]. Messenger RNA, peptidyl-tRNA, dipeptide, sordarin and ribosomal RNA modifications were built *de novo* in COOT. Several cycles of manual building in COOT and real space refinement in Phenix[56,57] were then performed for each model. Restraints were generated using the ELBOW algorithm integrated in the Phenix suite[58].

Model superimpositions and motion measurements

Models were superimposed using the *mmaker* command integrated in ChimeraX. Per-residue root mean square deviation (RMSD) values for individual chains were calculated in ChimeraX using the *rmsd* command. RMSD calculations of entire 40S subunits were performed in PyMOL using the *colorbyrmsd* script (The PyMOL Molecular Graphics System, Version 2.0 Schrödinger, LLC.). Rotation measurements and axis projections were generated using the *measure rotation* command in ChimeraX. Contact areas were quantified by applying the *measure buriedarea* command and default parameters for solvent-accessible surface calculations available through ChimeraX.

Data availability

Atomic coordinates and cryo-EM maps generated during this study are available through the Protein Data Bank (PDB) and the Electron Microscopy Databank (EMDB). The complexes have been deposited under following accession codes: PRE-H1 (8CCS, EMD-16563), PRE-H2 (8CDL, EMD- 16591), TI-1 (8CF5, EMD-16616), TI-2 (8CDR, EMD-16594), TI-3 (8CG8, EMD-16634), TI-4 (8CEH, EMD-16609), TI-5 (8CIV, EMD-16684), NR (8CGN, EMD-16648), TI-1* (8CKU, EMD-16702), TI-4* (8CMJ, EMD-16729).

References

35 Ben-Shem, A. *et al.* The structure of the eukaryotic ribosome at 3.0 A resolution. *Science* **334**, 1524-1529 (2011).

46 Pellegrino, S. *et al.* Structural Insights into the Role of Diphthamide on Elongation Factor 2 in mRNA Reading-Frame Maintenance. *J. Mol. Biol.* **430**, 2677-2687 (2018).

47 Jorgensen, R., Carr-Schmid, A., Ortiz, P. A., Kinzy, T. G. & Andersen, G. R. Purification and crystallization of the yeast elongation factor eEF2. *Acta Crystallogr. D Biol. Crystallogr.* **58**, 712-715 (2002).

48 Fraser, T. H. & Rich, A. Synthesis and aminoacylation of 3'-amino-3'-deoxy transfer RNA and its activity in ribosomal protein synthesis. *Proc. Natl. Acad. Sci. U. S. A.* **70**, 2671-2675 (1973).

49 Spirin, A. S., Belitsina, N. V. & Yusupova, G. Z. Ribosomal synthesis of polypeptides from aminoacyl-tRNA without polynucleotide template. *Methods Enzymol.* **164**, 631-649 (1988).

50 Mesters, J. R., Vorstenbosch, E. L. H., Deboer, A. J. & Kraal, B. Complete Purification of Transfer-Rna, Charged or Modified with Hydrophobic Groups, by Reversed-Phase High-Performance Liquid-Chromatography on a C-4 C-18 Column System. *J. Chromatogr. A* **679**, 93-98 (1994).

51 Mechulam, Y., Guillon, L., Yatime, L., Blanquet, S. & Schmitt, E. Protection-based assays to measure aminoacyl-tRNA binding to translation initiation factors. *Methods Enzymol.* **430**, 265-281 (2007).

52 Punjani, A., Rubinstein, J. L., Fleet, D. J. & Brubaker, M. A. cryoSPARC: algorithms for rapid unsupervised cryo-EM structure determination. *Nat Methods* **14**, 290-296 (2017).

53 Punjani, A. & Fleet, D. J. 3D variability analysis: Resolving continuous flexibility and discrete heterogeneity from single particle cryo-EM. *J. Struct. Biol.* **213**, 107702 (2021).

54 Goddard, T. D. *et al.* UCSF ChimeraX: Meeting modern challenges in visualization and analysis. *Protein Sci.* **27**, 14-25 (2018).

55 Pettersen, E. F. *et al.* UCSF ChimeraX: Structure visualization for researchers, educators, and developers. *Protein Sci.* **30**, 70-82 (2021).

56 Terwilliger, T. C. *et al.* Improved crystallographic models through iterated local density-guided model deformation and reciprocal-space refinement. *Acta Crystallogr. D Biol. Crystallogr.* **68**, 861-870 (2012).

57 Liebschner, D. *et al.* Macromolecular structure determination using X-rays, neutrons and electrons: recent developments in Phenix. *Acta Crystallogr D Struct Biol* **75**, 861-877 (2019).

58 Moriarty, N. W., Grosse-Kunstleve, R. W. & Adams, P. D. electronic Ligand Builder and Optimization Workbench (eLBOW): a tool for ligand coordinate and restraint generation. *Acta Crystallogr. D Biol. Crystallogr.* **65**, 1074-1080 (2009).

Acknowledgments

We are grateful to the staff of the Dubochet Centre for Imaging (DCI-Lausanne) for cryo-imaging and preliminary data analysis. We thank Dr. Yury Polikanov from the University of Illinois at Chicago for providing the plasmid for the over-expression of the CCA-adding enzyme. We also thank Corinne Crucifix from the IGBMC cryo-EM platform for her expertise in grid preparation. This work was supported by ”La Fondation pour la Recherche Médicale” DEQ20181039600 (to M.Y.).

Author contributions

M.Y. and G.Y conceived the project, N.M. conducted all biochemical experiments, N.M and A. M. collected cryo-EM data. Main data analysis was performed by N.M. L.J., and A.M. also contributed to the data analysis. N.M. prepared the manuscript. G.Y. reviewed and edited the

manuscript. G.Y. supervised the project. All authors gave their input in the preparation of the final manuscript.

Competing interests. The authors declare no competing interests.

Additional information

Correspondence and requests for materials should be addressed to G.Y. (email: gula@igbmc.fr)

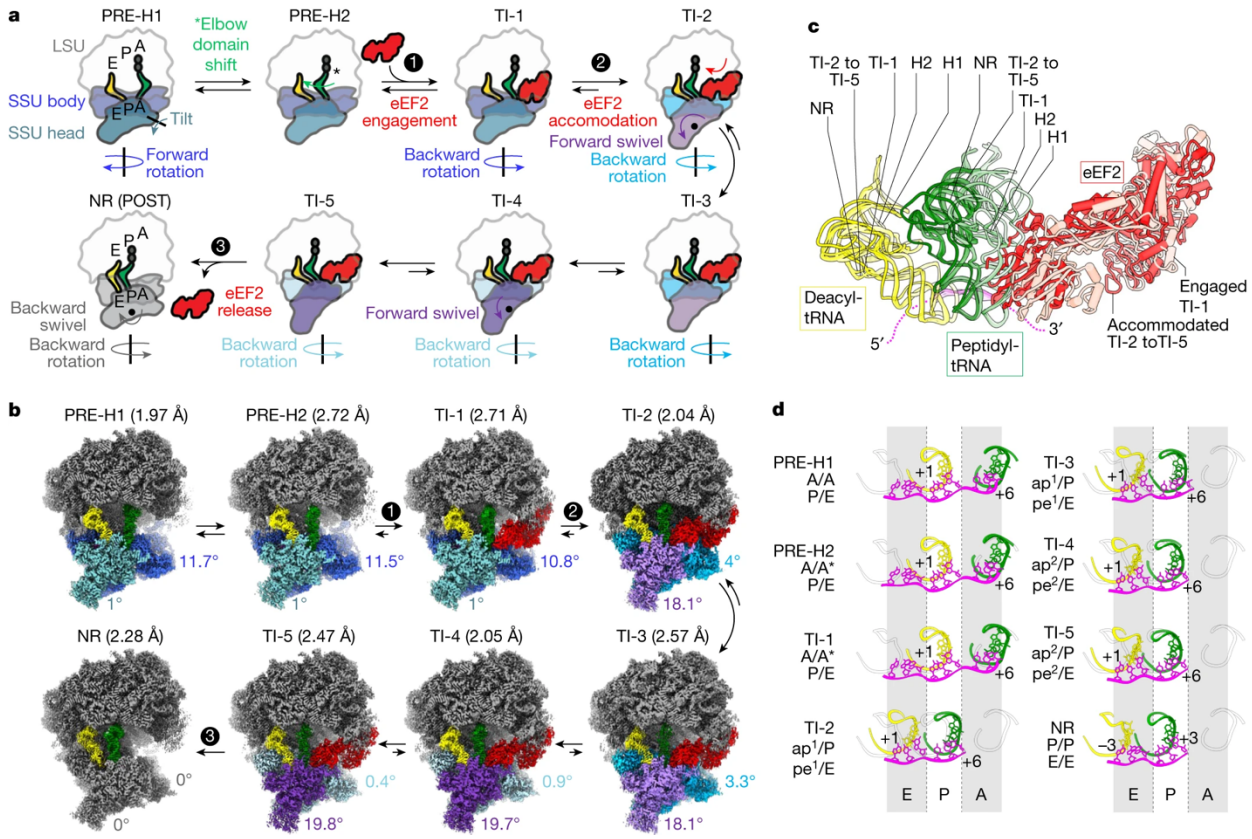
a
PRE-H1
*Elbow domain shift
PRE-H2
TI-1
TI-2
LSU
SSU body
SSU head
Tilt
Forward rotation
eEF2 engagement
Backward rotation
eEF2 accomodation
Forward swivel
Backward rotation
NR (POST)
TI-5
TI-4
TI-3
eEF2 release
Backward swivel
Backward rotation
Forward swivel
Backward rotation
Backward rotation
Backward rotation
b
PRE-H1 (1.97 Å)
PRE-H2 (2.72 Å)
TI-1 (2.71 Å)
TI-2 (2.04 Å)
11.7°
1°
11.5°
1°
10.8°
1°
4°
18.1°
NR (2.28 Å)
TI-5 (2.47 Å)
TI-4 (2.05 Å)
TI-3 (2.57 Å)
0°
0°
0.4°
19.8°
0.9°
19.7°
3.3°
18.1°
c
TI-2 to TI-5
TI-1
H2
H1
NR
TI-2 to TI-5
TI-1
H2
H1
NR
eEF2
Deacyl-tRNA
5′
Peptidyl-tRNA
3′
Engaged TI-1
Accommodated TI-2 toTI-5
d
PRE-H1 A/A P/E
PRE-H2 A/A* P/E
TI-1 A/A* P/E
TI-2 ap1/P pe1/E
TI-3 ap1/P pe1/E
TI-4 ap2/P pe2/E
TI-5 ap2/P pe2/E
NR P/P E/E
+1
+6
−3
+3
E
P
A

Fig. 1: Overview of eukaryotic ribosome translocation intermediates solved by cryo-EM

a, Schematic representation of eukaryotic translocation based on high-resolution cryo-EM reconstructions of elongating 80S ribosomal complexes reported in the current study. eEF2-catalyzed displacement of peptidyl- (green) and deacyl-tRNAs (yellow) from A to P, and P to E sites, respectively, is associated with SSU body domain back-rotation (dark blue to grey), and SSU head domain forward (cadet blue to violet) and backward swiveling (violet to grey). eEF2 is depicted in red, LSU is shown in grey, and dipeptide in dark grey. **b**, Overview of reported resolutions and cryo-EM maps, colored as in **a**. **c**, LSU alignment reveals tRNA translocation trajectories from PRE-H1 to NR depicted by light-to-dark palettes. TI-1 shows eEF2 in the recruitment phase (pink), while late translocation intermediates TI-2 to TI-5 reflect its fully accommodated state on the ribosome, e.g. TI-5 (red). mRNA is shown in magenta. **d**, Codon/anticodon duplex advancement displayed relative to PRE-H1 (A-site) and NR states (P- and E-sites). Alignment is performed on the SSU body domain.

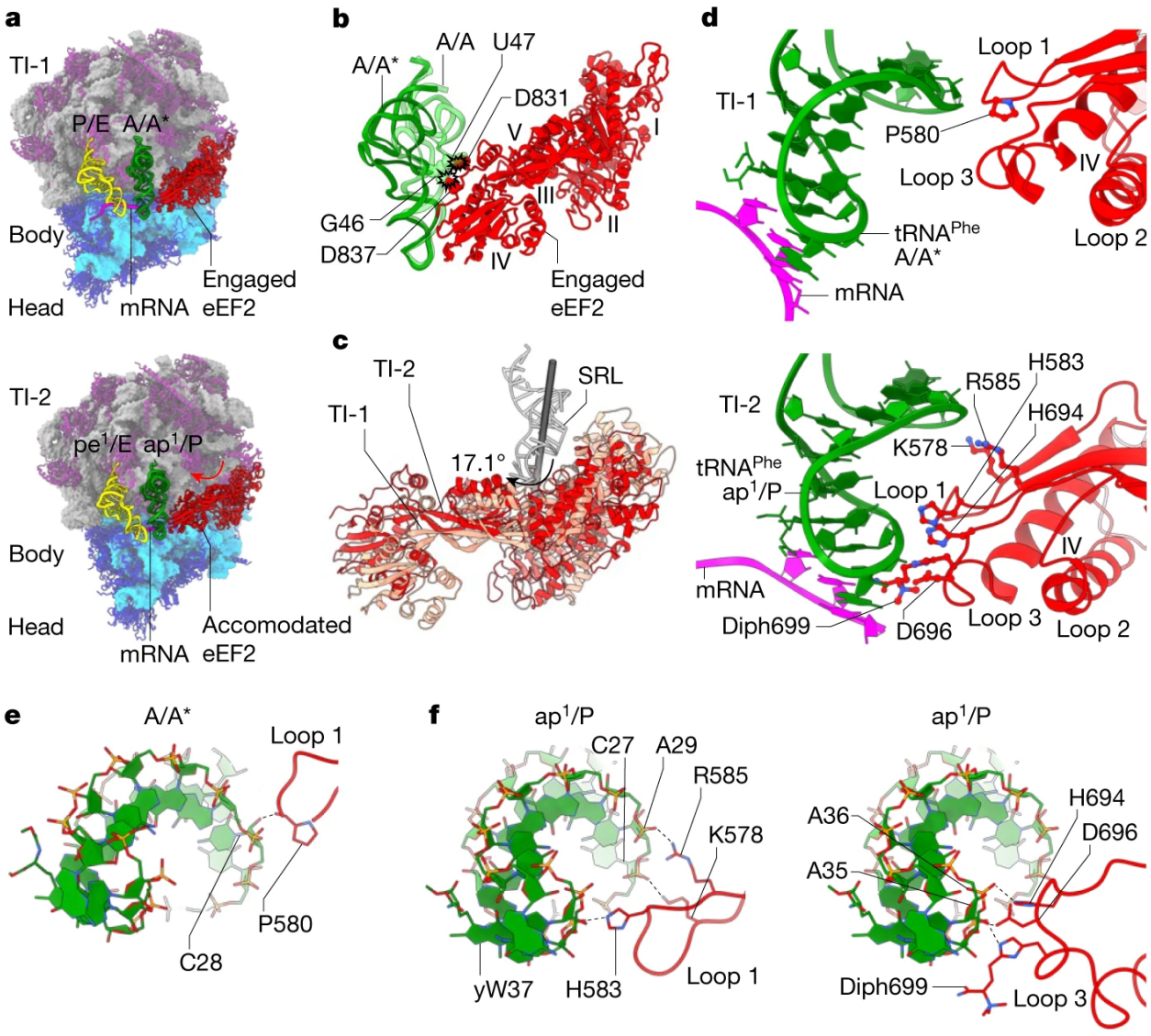
a
TI-1
P/E
A/A*
Body
Head
mRNA
Engaged
eEF2
TI-2
pe1/E
ap1/P
Body
Head
mRNA
Accomodated
eEF2
b
A/A
U47
A/A*
D831
V
I
III
II
G46
D837
IV
Engaged
eEF2
c
TI-2
SRL
TI-1
17.1°
d
Loop 1
TI-1
P580
Loop 3
IV
tRNAPhe
A/A*
Loop 2
mRNA
TI-2
H583
R585
H694
K578
tRNAPhe
ap1/P
Loop 1
IV
mRNA
Diph699
D696
Loop 3
Loop 2
e
A/A*
Loop 1
P580
C28
f
ap1/P
C27
A29
R585
K578
yW37
H583
Loop 1
ap1/P
H694
A36
D696
A35
Diph699
Loop 3

Fig. 2: eEF2 accommodation on the 80S ribosome and interactions of domain IV with ASL of peptidyl-tRNA in TI-1 and TI-2

a, Overview of TI-1 (top) and TI-2 (bottom) with peptidyl- (green) and deacyl-tRNAs (yellow), eEF2 (red) and messenger RNA (magenta). eEF2 accommodation on the 80S ribosome (red arrow) occurs as tRNAs advance from the hybrid A/A*-P/E to the chimeric ap^1/P-pe^1/E state. **b**, Shift of the peptidyl-tRNA elbow domain from A/A (light green) to A/A* (green) is required for eEF2 engagement on the 80S ribosome. Clashing residues of peptidyl-tRNA in the classical A/A state and eEF2 domain IV are displayed as ball models. **c**, Rotation of eEF2 around the sarcin-ricin loop (SRL) on its transition from the engaged to the accommodated state on the 80S ribosome. **d**, Residues of eEF2 domain IV stabilizing the ASL of peptidyl-tRNA in TI-1 (top) and in TI-2 (bottom). **e-f**, Per-loop interactions of eEF2 domain IV with ASLs of peptidyl tRNA in TI-1, in **e**, and TI-2, in **f**.

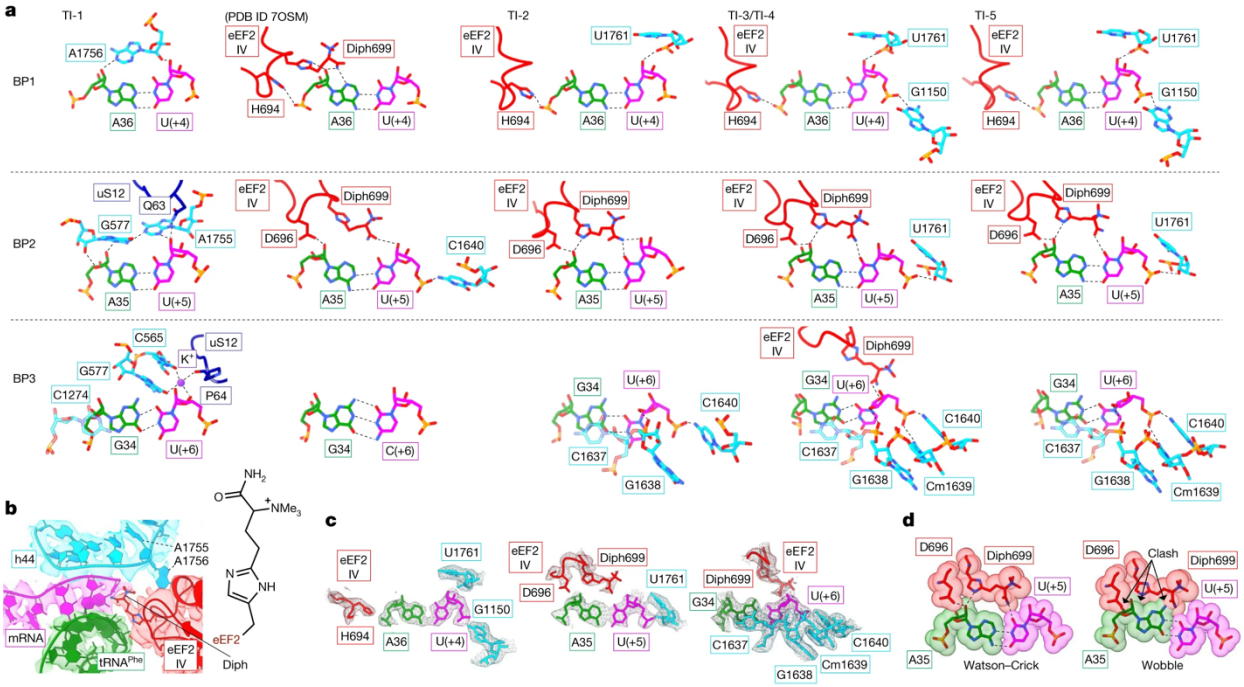
a
TI-1
(PDB ID 7OSM)
TI-2
TI-3/TI-4
TI-5
BP1
BP2
BP3
eEF2 IV
Diph699
A1756
A36
U(+4)
H694
U1761
G1150
uS12
Q63
G577
A1755
A35
U(+5)
D696
C1640
C565
K+
C1274
P64
G34
U(+6)
C(+6)
C1637
G1638
Cm1639
b
h44
A1755
A1756
mRNA
tRNAPhe
eEF2
Diph
NH2
NMe3
NH
c
d
Watson–Crick
Clash
Wobble

Fig. 3: Role of diphthamide in peptidyl-tRNA codon-anticodon stabilization

a, Interactions of codon-anticodon base pairs (BP) with residues of eEF2 domain IV (red), 18S ribosomal RNA (light blue) and the SSU protein uS12 (dark blue) observed in translocation intermediates TI-1 to TI-5 and in the previously reported early TI, PDB ID 7OSM. Conserved decoding nucleotides of TI-1 are in the fully locked conformation. Diphthamide stabilizes the second codon-anticodon BP in late translocation intermediates TI-2 to TI-5 and senses the third BP in TI-3 and TI-4. Top, middle and bottom panels correspond to first (BP1), second (BP2) and third base pairs (BP3), respectively. **b**, Close-up view of hypermodified residue diphthamide (Diph) of eEF2 domain IV (red) lying in the vicinity of the SSU helix 44 (light blue) and stabilizing the UUU codon of mRNA (magenta) and the GAA anticodon of fMet-Phe-N-tRNA^{Phe} (green), as observed in TI-2. Unfiltered, unsharpened density is contoured at σ = 3. **c**, Examples of cryo-EM density for BP1-BP3 and their interacting counterparts in the TI-4 complex shown at σ = 3. **d**, Diphthamide and aspartate residues of eEF2 domain IV impose steric restraints to the second codon-anticodon base pair and restrict Wobble geometry (e.g. TI-4). (See also Supplementary Video 3)

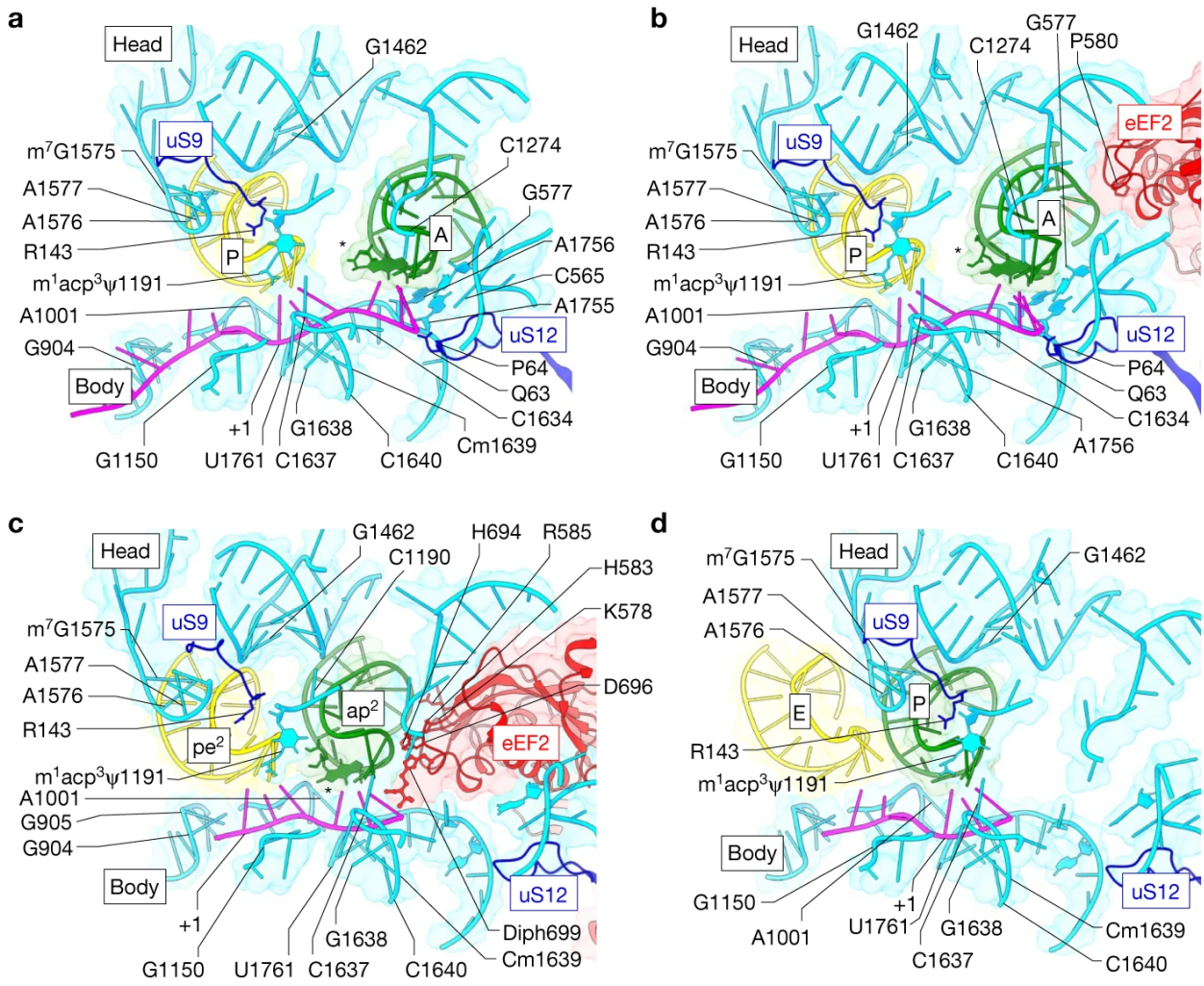
a
Head
G1462
uS9
m7G1575
C1274
A1577
G577
A1576
A
R143
P
A1756
m1acp3ψ1191
C565
A1755
A1001
uS12
G904
P64
Body
Q63
C1634
+1
G1638
Cm1639
G1150
U1761
C1637
C1640
b
Head
G1462
G577
C1274
P580
eEF2
m7G1575
uS9
A1577
A
A1576
R143
P
m1acp3ψ1191
A1001
uS12
G904
P64
Body
Q63
C1634
+1
G1638
A1756
G1150
U1761
C1637
C1640
c
Head
G1462
H694
R585
C1190
H583
m7G1575
uS9
K578
A1577
D696
A1576
ap2
R143
pe2
eEF2
m1acp3ψ1191
A1001
G905
G904
Body
uS12
+1
Diph699
G1638
Cm1639
G1150
U1761
C1637
C1640
d
m7G1575
Head
G1462
A1577
A1576
uS9
E
P
R143
m1acp3ψ1191
Body
uS12
G1150
+1
A1001
U1761
G1638
Cm1639
C1637
C1640

Fig. 4: mRNA-tRNA interactions with the SSU of the eukaryotic ribosome at different elongation states.

a-d, Interactions of mRNA (magenta) and ASLs of peptidyl- (green) and deacyl-tRNAs (yellow) with domain IV of eEF2 (red) and SSU body and head domains (18S in light blue and SSU proteins in dark blue). Movement of the mRNA-$tRNA_2$ module is shown for PRE-H1 in **a**, for TI-1 in **b**, for TI-4 in **c**, and NR in **d**. Annotations are displayed only for interacting residues. $tRNA^{Phe}$ hypermodification wybutosine (yW) at position 37 is marked with an asterisk.

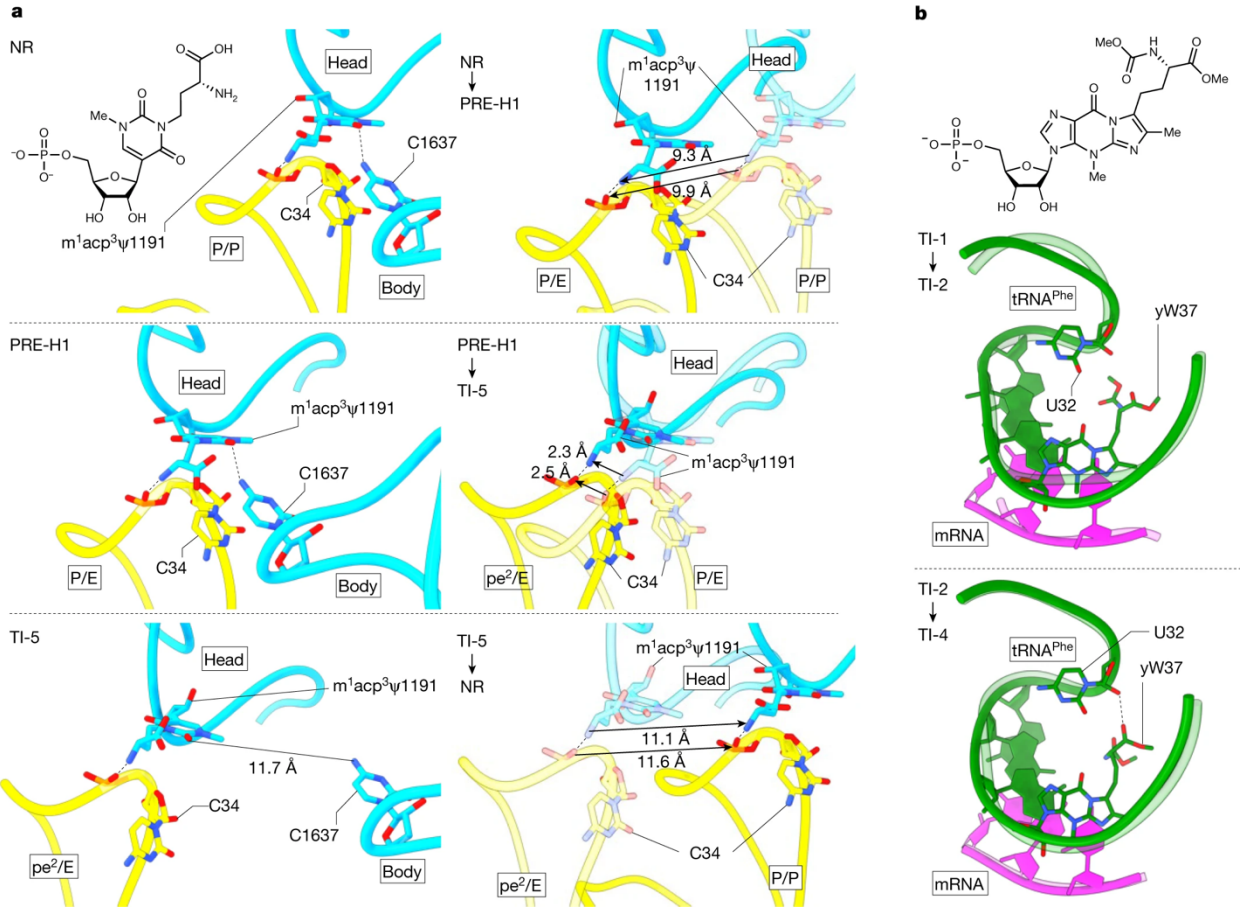
a
NR
Head
C1637
C34
P/P
Body
m1acp3ψ1191
NR
PRE-H1
m1acp3ψ
1191
Head
9.3 Å
9.9 Å
P/E
C34
P/P
PRE-H1
Head
m1acp3ψ1191
C1637
P/E
C34
Body
PRE-H1
TI-5
Head
2.3 Å
2.5 Å
m1acp3ψ1191
pe2/E
C34
P/E
TI-5
Head
m1acp3ψ1191
11.7 Å
C34
C1637
pe2/E
Body
TI-5
NR
m1acp3ψ1191
Head
11.1 Å
11.6 Å
C34
pe2/E
P/P
b
MeO
OMe
Me
Me
HO
OH
TI-1
TI-2
tRNAPhe
yW37
U32
mRNA
TI-2
TI-4
tRNAPhe
U32
yW37
mRNA

Fig. 5: Role of *S. cerevisiae* hypermodifications $m^1acp^3\Psi1191$ of 18S and wybutosine (yW37) of $tRNA^{Phe.}$

a, Base-unspecific hydrogen bond interactions between hypermodified 1-methyl-3-α-amino-α-carboxyl-propyl pseudouridine ($m^1acp^3\Psi1191$) and the first anticodon nucleotide C34 of deacyl-$tRNA^{fMet}$ (yellow) are shown for NR, PRE-H1 and TI-5 states (left). In NR and early translocation intermediates (e.g. PRE-H1), $m^1acp^3\Psi1191$ interacts with the SSU body residue C1637, compatible with non-swiveled conformations of the SSU head. Swiveled conformations of the SSU head domain in late translocation intermediates (e.g. TI-5) break the contact between $m^1acp^3\Psi1191$ and C1637. Respective transitions between NR, PRE-H1 and TI-5 states (right) reveal that the $m^1acp^3\Psi1191$ platform guides deacyl-$tRNA^{fMet}$ anticodon translocation by fixing and moving C34 from P- towards the E-site, after which the anticodon is released and the hypermodification fixes the next P-site anticodon. **f**, Bulky chain of yW37 protrudes into the anticodon stem loop (ASL) and forms a hydrogen bond with U32 in TI-4. ASL alignments of fMet-Phe-$tRNA^{Phe}$ (residues 27-43) during transitions from TI-1 to TI-2, and from TI-2 to TI-4 reveal intramolecular remodeling of the $tRNA^{Phe}$ ASL (white arrows). (See also Supplementary Video 5)

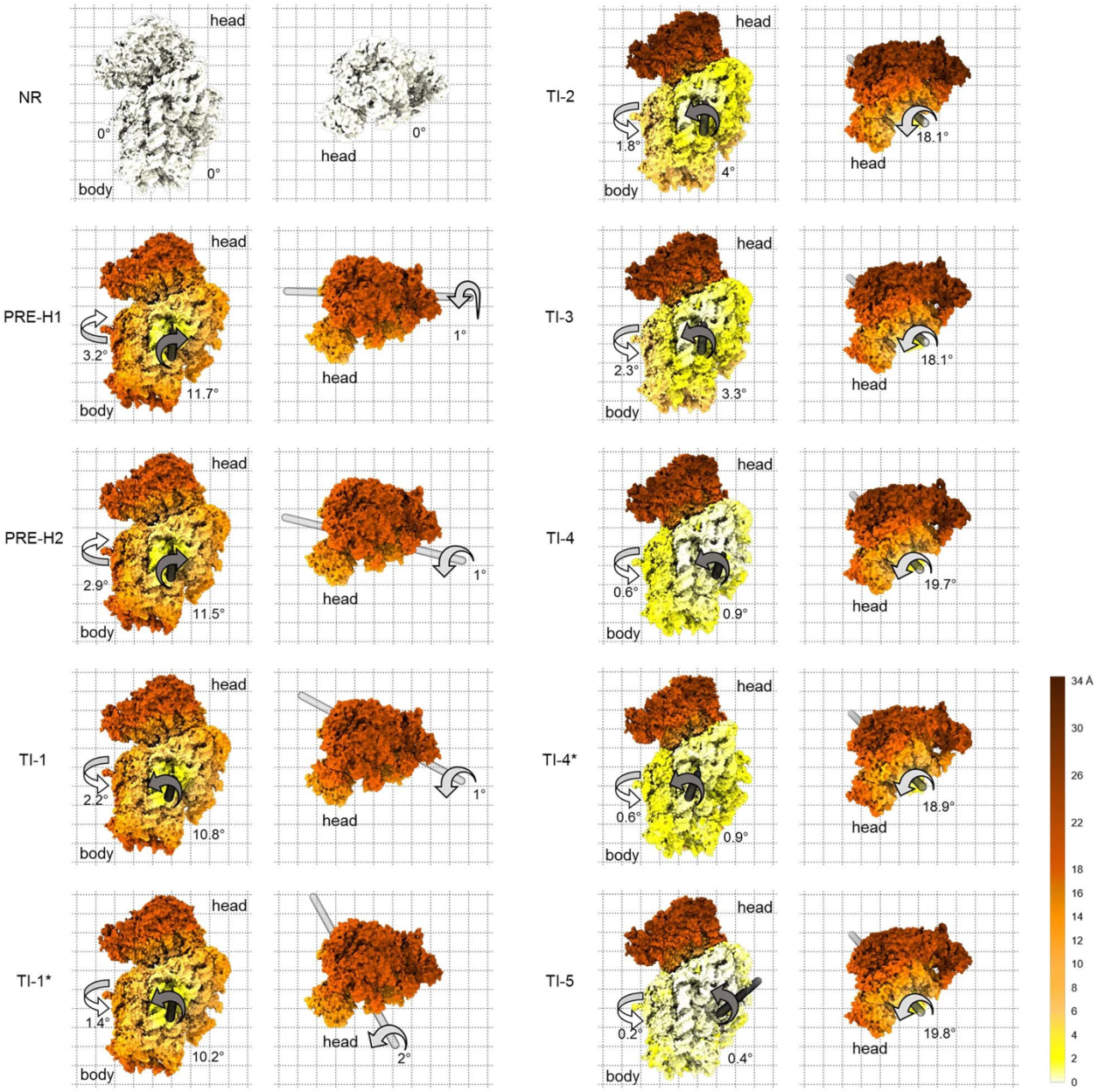
NR
head
0°
0°
body
0°
head
TI-2
head
1.8°
4°
body
18.1°
head
PRE-H1
head
3.2°
11.7°
body
1°
head
TI-3
head
2.3°
3.3°
body
18.1°
head
PRE-H2
head
2.9°
11.5°
body
1°
head
TI-4
head
0.6°
0.9°
body
19.7°
head
TI-1
head
2.2°
10.8°
body
1°
head
TI-4*
head
0.6°
0.9°
body
18.9°
head
TI-1*
head
1.4°
10.2°
body
head
2°
TI-5
head
0.2°
0.4°
body
19.8°
head
34 Å
30
26
22
18
16
14
12
10
8
6
4
2
0

Extended Data Fig. 1: Large-scale conformational changes of the small ribosomal subunit.

Intersubunit view of the full SSU (left grid) and a zoomed top view of the SSU head domain (right grid) for each solved translocation complex. SSU is coloured on the basis of root-mean-square deviation values of atomic positions relative to the non-rotated (NR) state by 25S alignment. White arrows indicate shoulder domain closure (upwards) or opening (downwards). Dark grey arrows indicate small subunit rotation (clockwise) or back-rotation (anti-clockwise) around the rotation axes shown in black. Light grey arrows indicate forward tilting or swiveling motions around the axes shown in light gray. All angles are calculated relative to the NR state.

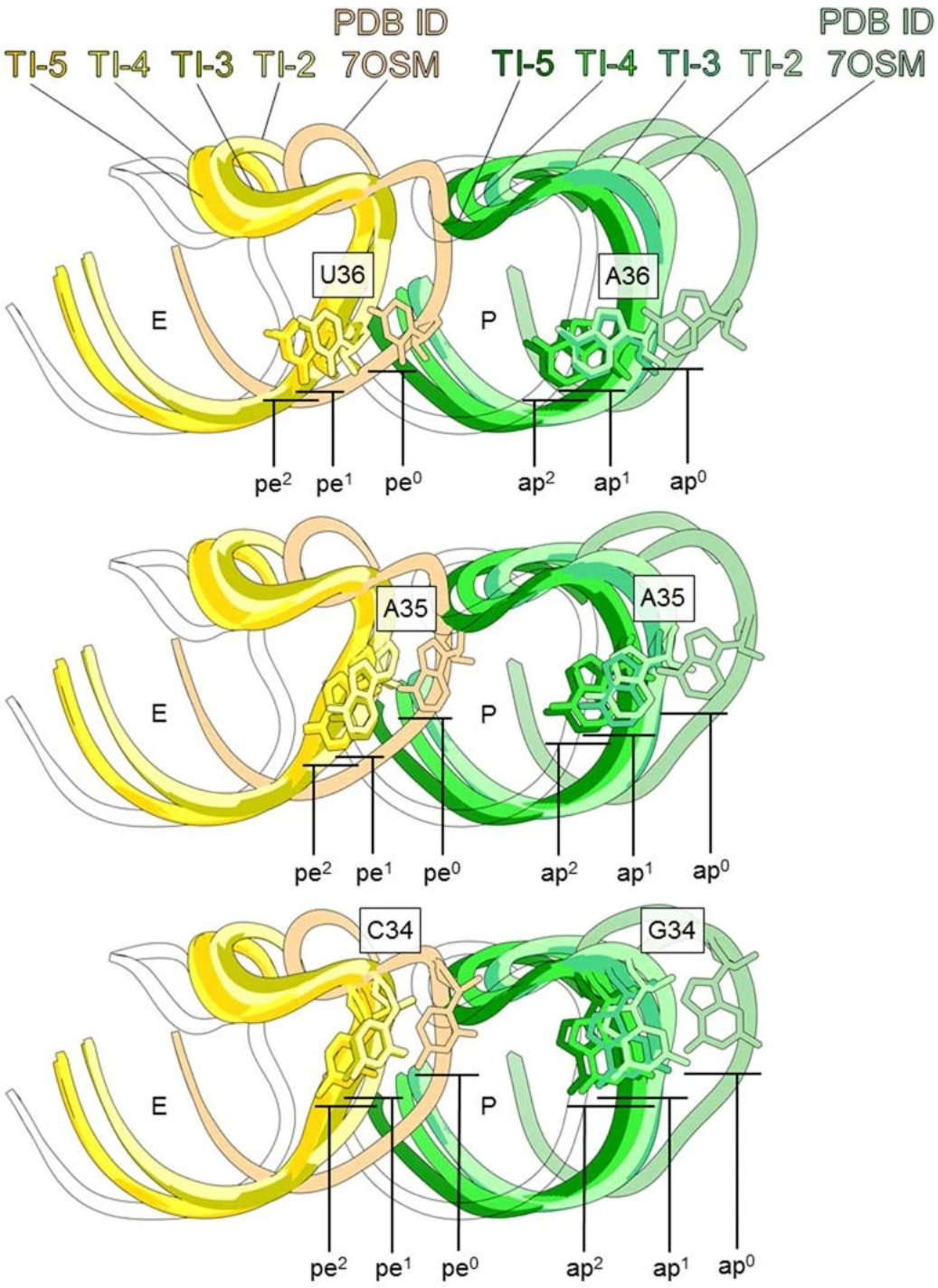
PDB ID
TI-5 TI-4 TI-3 TI-2 7OSM
PDB ID
TI-5 TI-4 TI-3 TI-2 7OSM
U36
A36
E
P
pe2 pe1 pe0 ap2 ap1 ap0
A35
A35
E
P
pe2 pe1 pe0 ap2 ap1 ap0
C34
G34
E
P
pe2 pe1 pe0 ap2 ap1 ap0

Extended Data Fig. 2: Progressive anticodon advancement in chimeric states of translocation.

Positions of peptidyl- (green) and deacyl-tRNA (yellow) anticodons in chimeric states of translocation TI-2 to TI-5 relative to final positions observed in the NR state (white) and the early chimeric ap^0/P-pe^0/E state (PDB ID 7OSM). Individually displayed anticodon nucleotides (top to bottom in the 3' – 5' direction) reveal distinct SSU sub-chimeric states: ap^1-pe^1 (in TI-2 and TI-3) and ap^2-pe^2 (in TI-4 and TI-5).

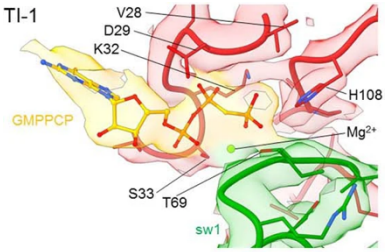
TI-1
V28
D29
K32
H108
GMPPCP
Mg2+
S33
T69
sw1

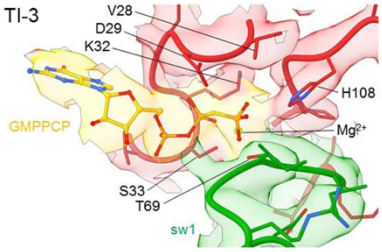
TI-3
V28
D29
K32
H108
GMPPCP
Mg2+
S33
T69
sw1

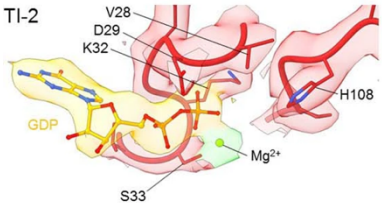
TI-2
V28
D29
K32
H108
GDP
Mg2+
S33

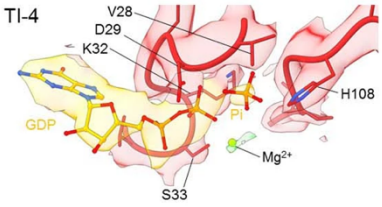
TI-4
V28
D29
K32
H108
GDP
Pi
Mg2+
S33

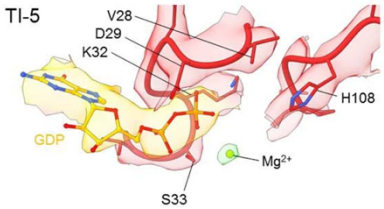
TI-5
V28
D29
K32
H108
GDP
Mg2+
S33

Extended Data Fig. 3: Nucleotide-binding pockets of eEF2 in translocation intermediates from TI-1 to TI-5.

Unfiltered, unsharpened maps (σ=3) of the nucleotide-binding pocket found in domain I of eEF2 (red). TI-1 and TI-3 show density for the non-hydrolysable analogue of GTP (GMPPCP) and switch loop 1 (sw1). GDP-containing TI-2, TI-4 and TI-5 show no density for sw1. Additional density corresponding to inorganic phosphate was identified in TI-4.

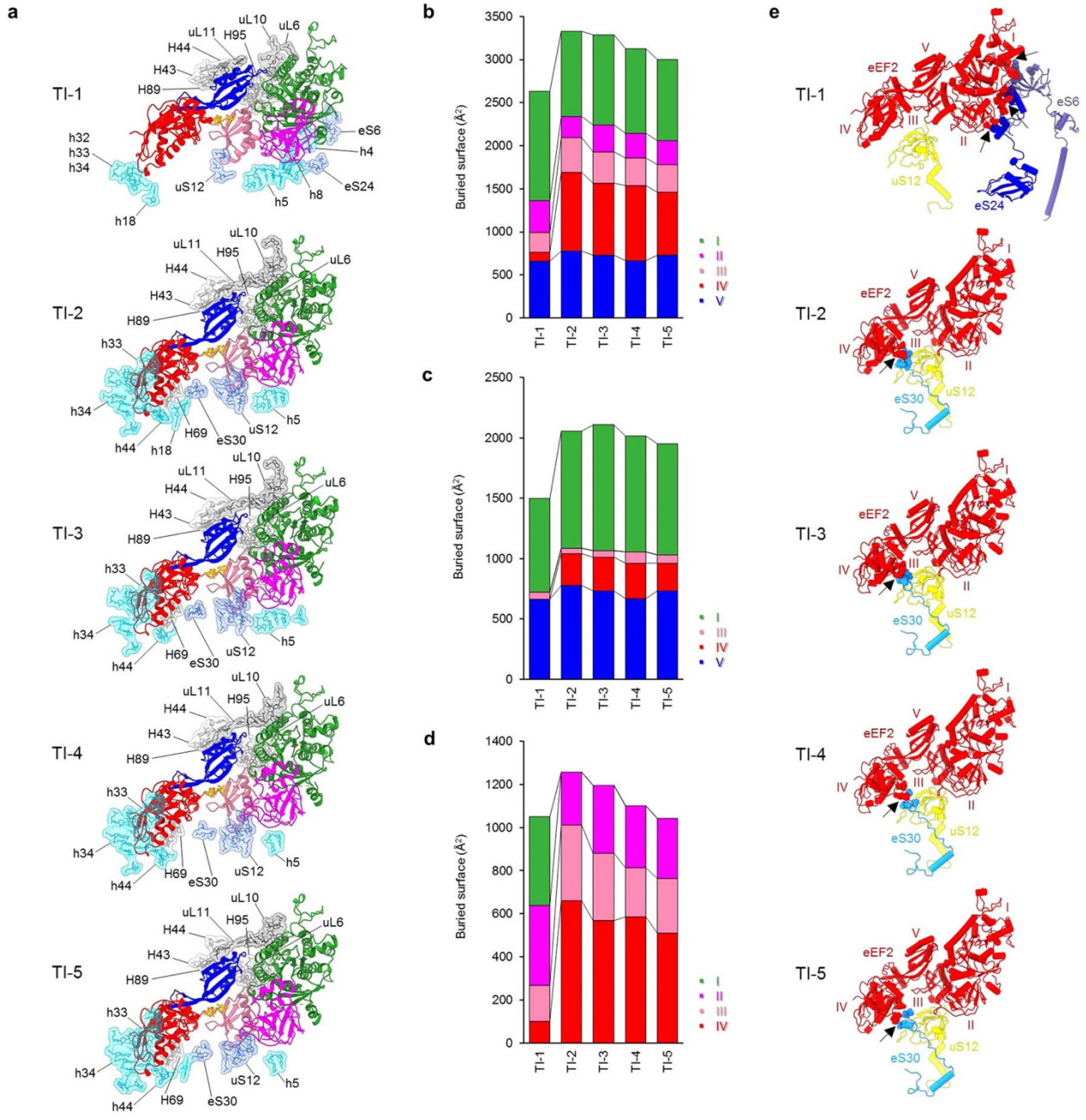
a
TI-1
TI-2
TI-3
TI-4
TI-5
uL10
uL11
uL6
H95
H44
H43
H89
h32
h33
h34
eS6
h4
uS12
h5
h8
eS24
h18
H69
eS30
h44
b
Buried surface (Å²)
3500
3000
2500
2000
1500
1000
500
0
I
II
III
IV
V
c
d
1400
1200
1000
800
600
400
200
e
eEF2
eS6
eS24
uS12
eS30

Extended Data Fig. 4: eEF2 interactions with the eukaryotic 80S ribosome.

a, Contacts of eEF2 domains (I in green, II in magenta, III in pink, IV in red, and V in blue) with ribosomal elements of large 60S (RNA in light grey and proteins in dark grey) and small 40S subunit (RNA in light blue and proteins in dark blue) in translocation intermediate complexes TI-1 to TI-5. Sordarin is depicted in orange. **b-d**, Quantification of contact areas of eEF2 domains I to V with 80S, in **b**, large 60S subunit, in **c**, and small 40S subunit, in **d**. Eukaryote-specific interactions between eEF2 and SSU proteins eS6 and eS24 during factor recruitment in early translocation (TI-1), and eS30 once eEF2 is fully accommodated on 80S (TI-2 to TI-5). Black arrows indicate areas of eukaryote-specific contacts.

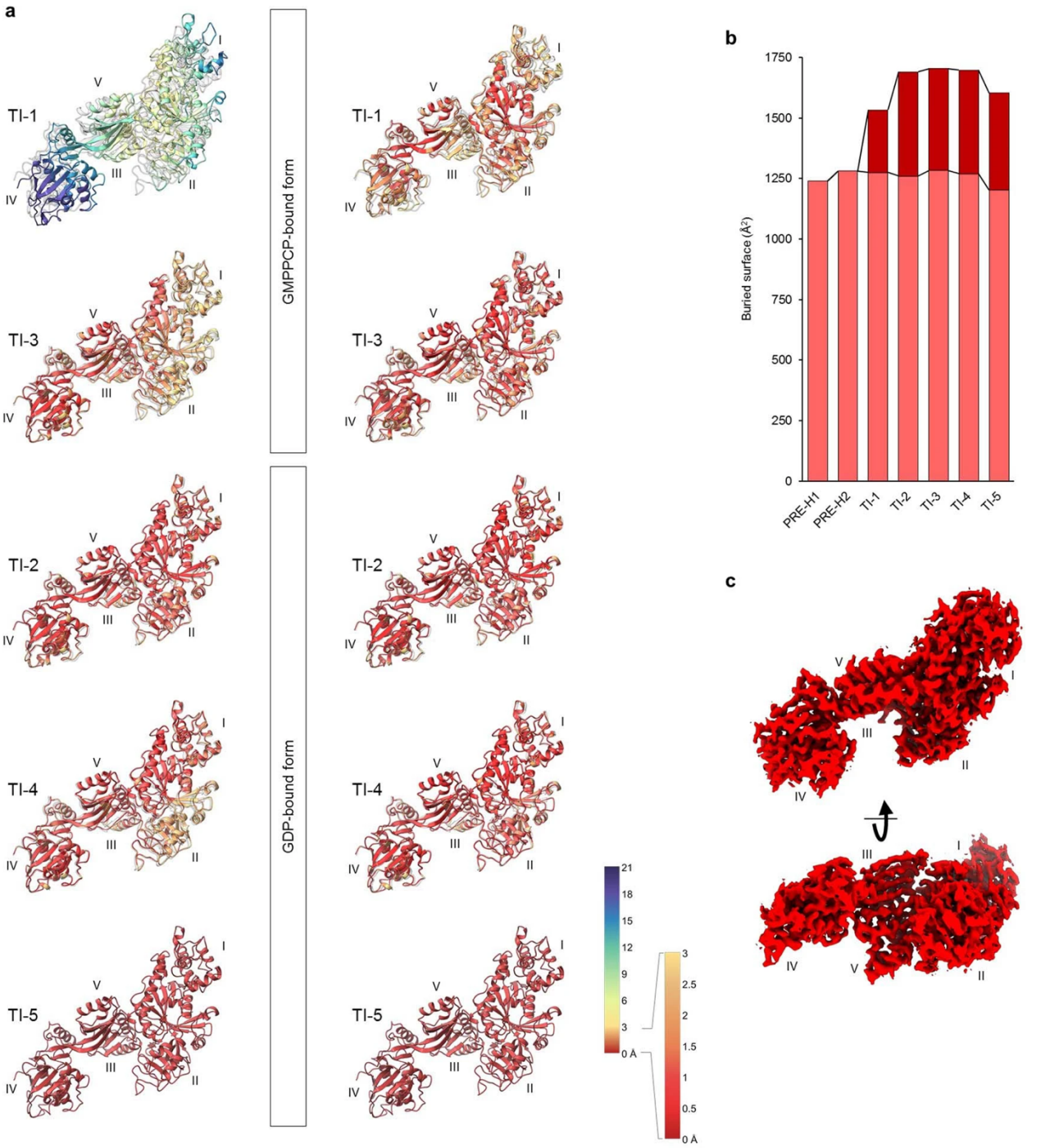
a
TI-1
TI-3
TI-2
TI-4
TI-5
I
II
III
IV
V
GMPPCP-bound form
GDP-bound form
21
18
15
12
9
6
3
0 Å
3
2.5
2
1.5
1
0.5
0 Å
b
Buried surface (Å²)
1750
1500
1250
1000
750
500
250
0
PRE-H1
PRE-H2
TI-1
TI-2
TI-3
TI-4
TI-5
c

Extended Data Fig. 5: Conformational adaptations of eEF2 and contact areas with the $tRNA_2$-mRNA translocating module.

a, Alignment on 25S (left) and global eEF2 alignment (right) on eEF2 in TI-5 for GMPPCP bound intermediates TI-1 and TI-3, and GDP-containing intermediates TI-2, TI-4 and TI-5. Atoms are colored on the basis of root-mean-square deviation values of atomic positions relative to TI-5. **b**, Buried surface measurements corresponding to contacts of the $tRNA_2$-mRNA module with 80S ribosome (pink) and domain IV of eEF2 (red) in the course of elongation from PRE-H1 to TI-5. **c**, Unfiltered, unsharpened density of *S. cerevisiae* eEF2 (e.g. TI-4) contoured at $\sigma = 3$.

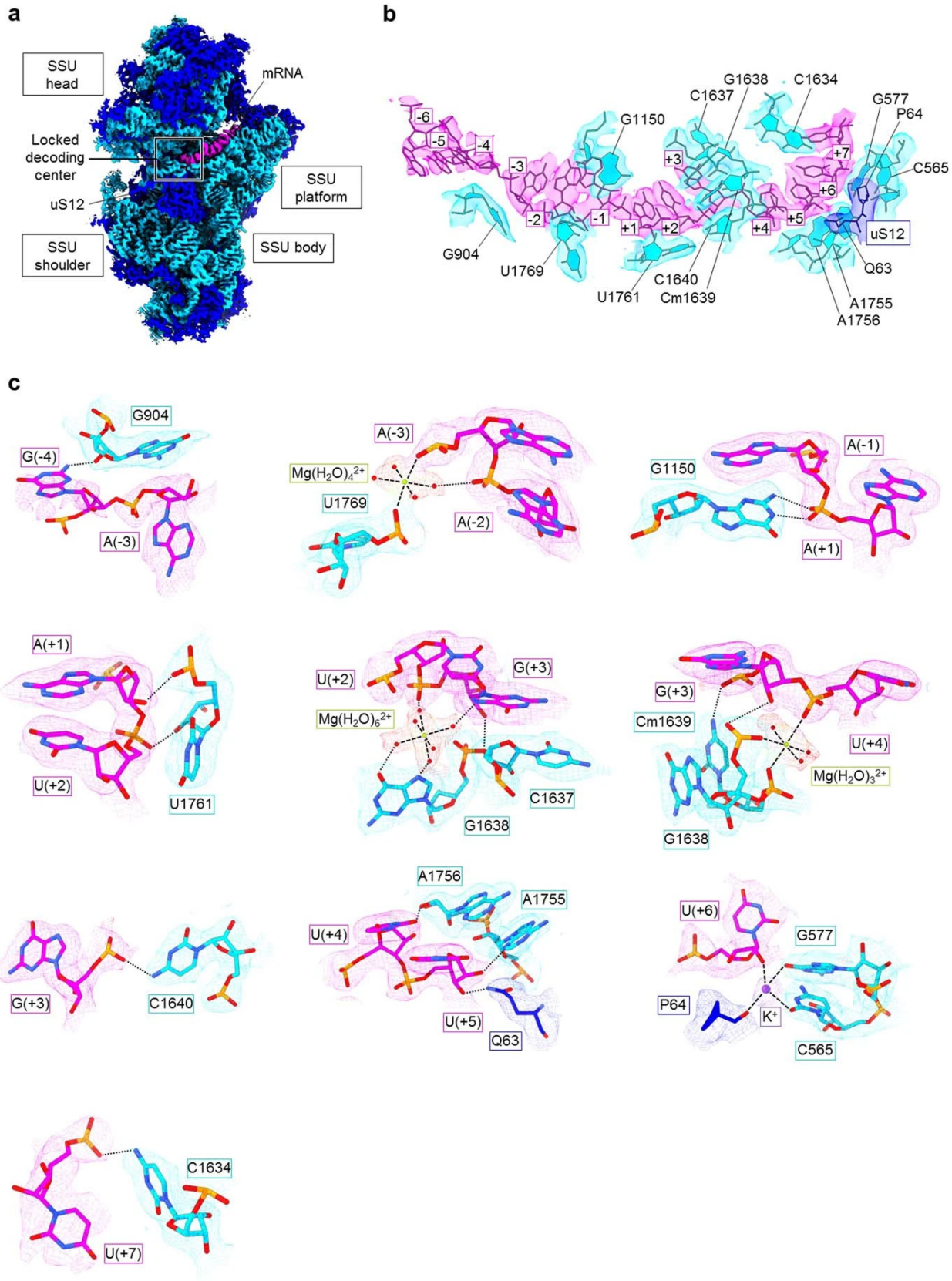
a
SSU head
mRNA
Locked decoding center
SSU platform
uS12
SSU shoulder
SSU body
b
G1638
C1634
C1637
G577
P64
G1150
-6
-5
-4
-3
+3
+7
C565
+6
-2
-1
+1
+2
+4
+5
uS12
G904
U1769
C1640
Cm1639
U1761
Q63
A1755
A1756
c
G904
G(-4)
A(-3)
A(-3)
Mg(H2O)4 2+
U1769
A(-2)
A(-1)
G1150
A(+1)
A(+1)
U(+2)
U1761
U(+2)
G(+3)
Mg(H2O)6 2+
C1637
G1638
G(+3)
Cm1639
U(+4)
Mg(H2O)3 2+
G1638
A1756
A1755
U(+4)
U(+5)
Q63
G(+3)
C1640
U(+6)
G577
P64
K+
C565
C1634
U(+7)

Extended Data Fig. 6: mRNA path on the small subunit of the eukaryotic 80S ribosome
a, Lateral view of the full 40S small subunit (SSU) of the eukaryotic 80S ribosome trapped in the PRE-hybrid-1 reconstruction (PRE-H1) reveals the path of messenger RNA (magenta) at the SSU head-body domain interface. Unsharpened, unfiltered high-resolution cryo-EM maps are shown at σ = 3.5. 18S ribosomal RNA and SSU proteins are colored in light and dark blue, respectively. **b**, Zoom on the thirteen nucleotide-long messenger RNA and interacting residues of 18S rRNA and the conserved SSU protein uS12. +1 indicates the first nucleotide of the start codon. **c**, Close-up view of the interactions between messenger RNA and ribosomal SSU elements in the PRE-H1 complex. π-π stacking is found between -1 and G1150, while the p-π effect is observed in the following interacting pairs: -3 and G904, and +3 and C1637.

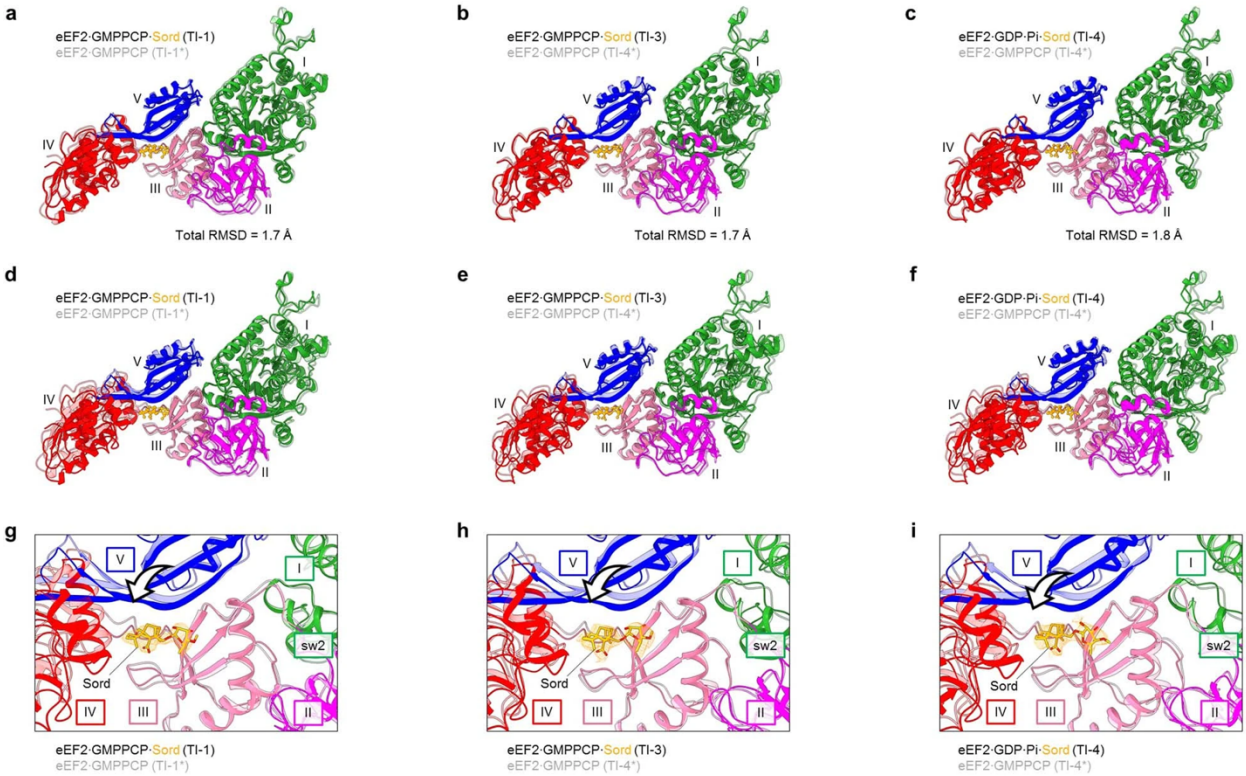

j

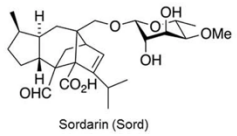

Sordarin (Sord)

Extended Data Fig. 7: Effect of sordarin binding to eEF2 in the context of eukaryotic translocation

a-c, Global alignments reflecting general conservation of overall eEF2 conformation during early, in **a**, and late states of translocation, in **b** and **c**. **d-f**, Domain III alignment shows displacement of eEF2 domain V towards the interface with domain III. **g-I**, Zoom on the sordardin binding site for respective structural superimpositions on eEF2 domain III, as shown in **d-f**. The arrow indicates the displacement of domain V relative to domain III. Remodeling of the switch loop 2 (sw2) has not been observed. Structural alignments are performed for late translocation states before, in **b**, **e** and **h,** and after GTP hydrolysis, in **c**, **f** and **i**. eEF2 domains are colored as follows: domain I in green, domain II in magenta, domain III in pink, domain IV in red, and domain V in blue. Unfiltered, unsharpened of sordarin is shown at $\sigma = 4$ and depicted in orange. Lighter nuances correspond to structures without sordardin, TI-1* and TI-4*. **j**, Chemical structure of sordarin.

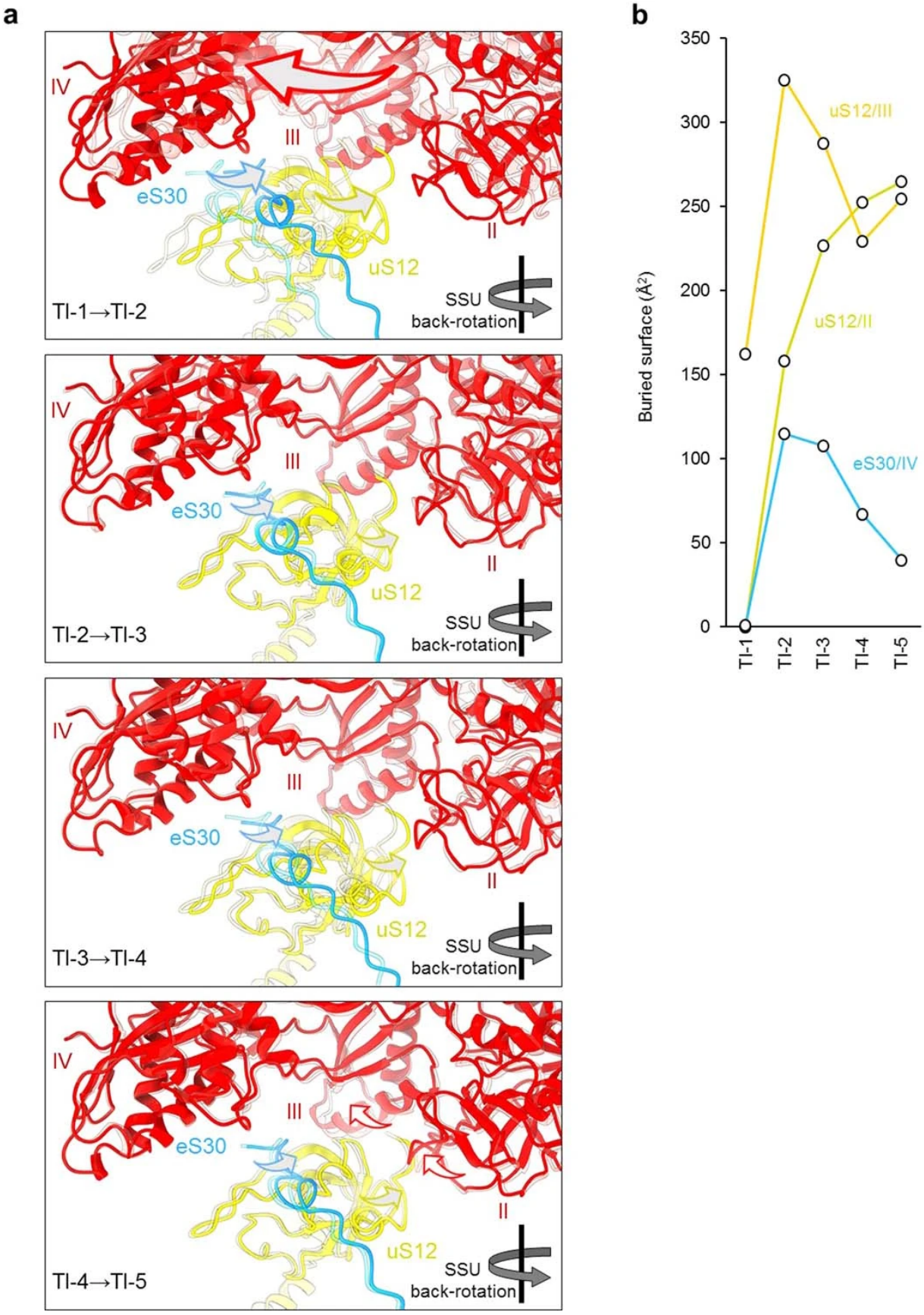
a
IV
III
eS30
II
uS12
SSU
back-rotation
TI-1→TI-2
TI-2→TI-3
TI-3→TI-4
TI-4→TI-5
b
Buried surface (Å²)
350
300
250
200
150
100
50
0
uS12/III
uS12/II
eS30/IV
TI-1
TI-2
TI-3
TI-4
TI-5

Extended Data Fig. 8: Interactions of eEF2 with small subunit proteins uS12 and eS30

a, Inter-domain remodeling of eEF2 and conformational changes of SSU proteins uS12 and eS30 accompanying SSU back-rotation during respective transitions between translocation intermediates TI-1 to TI-5. **b**, Curves depicting contacts between SSU proteins uS12 with eEF2 domains II (dark yellow) and III (orange), and eS30 with domain IV (blue).

	Non-rotated	PRE-H1	TI-2	TI-4	TI-5
PDB	8CGN	8CCS	8CDR	8CEH	8CIV
EMDB	EMD-16648	EMD-16563	EMD-16594	EMD-16609	EMD-16684
Grid					
Manufacturer	Quantifoil	Quantifoil	Quantifoil	Quantifoil	Quantifoil
Type	Ultrathin Carbon	Ultrathin Carbon	Ultrathin Carbon	Ultrathin Carbon	Ultrathin Carbon
Hole size/spacing	R 2/2	R 2/2	R 2/2	R 2/2	R 2/2
Mesh	300 (Au)	300 (Au)	300 (Au)	300 (Au)	300 (Au)
Sample					
Volume (µl)	3	3	3	3	3
Concentration (µM)	0.1	0.1	0.1	0.1	0.1
Blot time (s)	4	4	4	4	4
Temperature (°C)	9	9	9	9	9
Humidity (%)	95	95	95	95	95
Data collection and processing					
Microscope	Titan Krios G4	Titan Krios G4	Titan Krios G4	Titan Krios G4	Titan Krios G4
Electron source	E-CFEG	E-CFEG	E-CFEG	E-CFEG	E-CFEG
Acceleration voltage (keV)	300	300	300	300	300
Camera	Falcon 4	Falcon 4	Falcon 4	Falcon 4	Falcon 4
Nominal magnification	270,000	270,000	270,000	270,000	270,000
Pixel size	0.452	0.452	0.452	0.452	0.452
Total electron exposure (e^{-}/Å^2)	60	60	60	60	60
C2 aperture diameter (µm)	50	50	50	50	50
Nominal minimum defocus (nm)	400	400	400	400	400
Nominal maximum defocus (nm)	1,000	1,000	1,000	1,000	1,000
Number of collected micrographs	47,618	47,618	47,618	47,618	47,618
Number of used micrographs	45,282	45,282	45,282	45,282	45,282
Total number of extracted particles	616,978	616,978	616,978	616,978	616,978
Number of refined particles	442,508	442,508	442,508	442,508	442,508
Final number of complex particles	21,458	55,455	58,351	55,762	23,773
Resolution, unsharpened (Å)	2.28	1.97	2.04	2.05	2.47
FSC threshold	0.143	0.143	0.143	0.143	0.143
Model-to-map					
CC mask	0.81	0.85	0.84	0.85	0.84
CC volume	0.81	0.85	0.84	0.85	0.83
Resolution (Å)	2.64	2.23	2.40	2.41	2.82
FSC threshold	0.5	0.5	0.5	0.5	0.5
Model					
Atoms	201,528	201,697	207,753	207,126	207,374
Nucleotide residues	5,257	5,236	5,241	5,241	5,256
Protein residues	11,089	11,130	11,910	11,848	11,848
Bonds (RMSD)					
Length (Å)	0.003	0.005	0.007	0.008	0.009
Angles (°)	0.750	0.806	0.751	0.802	0.845
MolProbity score	2.09	2.14	2.14	2.20	2.10
Clash score	10.82	9.68	10.41	11.03	11.21
Ramachandran plot					
Outliers	0.02	0.08	0.02	0.05	0.05
Allowed	3.52	4.05	3.21	3.68	3.20
Favored	96.46	95.87	96.77	96.26	96.75
Ramachandran plot Z-score, whole	-0.73	-0.87	-0.87	-1.86	-0.85
Rotamer outliers (%)	2.55	2.81	3.34	3.25	2.76
Cβ outliers (%)	0.00	0.00	0.00	0.00	0.00
CαBLAM outliers (%)	4.19	4.14	4.06	4.40	4.16
ADP B factors, mean (Å^2)					
Protein	62.17	57.88	64.08	69.57	60.91
Nucleotide	59.49	53.20	58.61	64.61	58.18

Extended Data Table. 1: Grid preparation, data collection and model validation parameters for NR, PRE-H1, TI-2, TI-4 and TI-5 complexes.

	TI-1	TI-3	PRE-H2	TI-1*	TI-4*
PDB	8CF5	8CG8	8CDL	8CKU	8CMJ
EMDB	EMD-16616	EMD-16634	EMD-16591	EMD-16702	EMD-16729
Grid					
Manufacturer	Quantifoil	Quantifoil	Quantifoil	Quantifoil	Quantifoil
Type	Ultrathin Carbon	Ultrathin Carbon	Ultrathin Carbon	Ultrathin Carbon	Ultrathin Carbon
Hole size/spacing	R 2/2	R 2/2	R 2/2	R 2/2	R 2/2
Mesh	300 (Au)	300 (Au)	300 (Au)	300 (Au)	300 (Au)
Sample					
Volume (µl)	3	3	3	3	3
Concentration (µM)	0.1	0.1	0.1	0.1	0.1
Blot time (s)	4	4	4	4	4
Temperature (°C)	9	9	9	9	9
Humidity (%)	95	95	95	95	95
Data collection					
Microscope	Titan Krios G4	Titan Krios G4	Titan Krios G4	Titan Krios G4	Titan Krios G4
Electron source	E-CFEG	E-CFEG	E-CFEG	E-CFEG	E-CFEG
Acceleration voltage (keV)	300	300	300	300	300
Camera	Falcon 4	Falcon 4	Falcon 4	Falcon 4	Falcon 4
Nominal magnification	270,000	270,000	165,000	165,000	165,000
Pixel size	0.452	0.452	0.726	0.726	0.726
Total electron exposure ($e^-/Å^2$)	40	40	40	40	40
C2 aperture diameter (µm)	50	50	50	50	50
Nominal minimum defocus (nm)	400	400	400	400	400
Nominal maximum defocus (nm)	1,000	1,000	1,000	1,000	1,000
Number of collected micrographs	42,262	42,262	16,683	16,683	16,683
Number of used micrographs	39,533	39,533	16,654	16,654	16,654
Total number of extracted particles	514,460	514,460	624,552	624,552	624,552
Number of refined particles	393,786	393,789	561,498	561,498	561,498
Final number of complex particles	23,096	73,086	68,945	22,551	41,878
Resolution, unsharpened (Å)	2.71	2.57	2.72	3.11	3.79
FSC threshold	0.143	0.143	0.143	0.143	0.143
Model-to-map					
CC mask	0.83	0.80	0.85	0.79	0.73
CC volume	0.81	0.79	0.84	0.78	0.73
Resolution (Å)	2.96	2.96	2.99	3.62	4.63
FSC threshold	0.5	0.5	0.5	0.5	0.5
Model					
Atoms	208,161	207,325	201,553	207,340	202,630
Nucleotide residues	5,236	5,240	5,237	5,236	5,081
Protein residues	11,977	11,874	11,130	11,975	11,845
Bonds (RMSD)					
Length (Å)	0.008	0.07	0.04	0.06	0.004
Angles (°)	0.840	0.755	0.758	0.903	0.881
MolProbity score	1.90	1.83	1.80	1.95	2.07
Clash score	12.99	13.55	11.08	17.80	23.23
Ramachandran plot					
Outliers	0.09	0.02	0.06	0.03	0.04
Allowed	3.89	3.15	3.52	3.23	3.28
Favored	96.02	96.84	96.42	96.73	96.68
Ramachandran plot Z-score, whole	-0.91	-1.26	-0.70	-1.07	-1.54
Rotamer outliers (%)	0.25	0.05	0.17	0.05	0.04
Cβ outliers (%)	0.00	0.00	0.00	0.00	0.01
CαBLAM outliers (%)	3.99	4.22	4.12	4.17	4.31
ADP B factors, mean ($Å^2$)					
Protein	54.45	62.40	80.47	86.61	126.50
Nucleotide	60.62	64.49	74.57	88.28	124.64

Extended Data Table. 2: Grid preparation, data collection and model validation parameters for TI-1, TI-3, PRE-H2, TI-1* and TI-4* complexes.

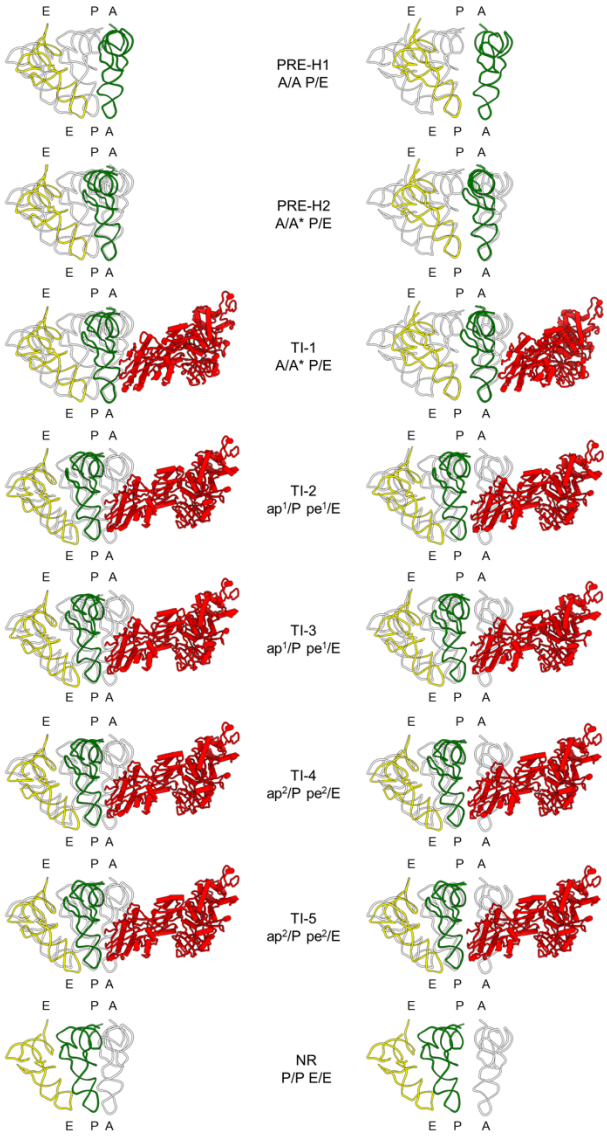
E P A
PRE-H1
A/A P/E
E P A
E P A
PRE-H2
A/A* P/E
E P A
E P A
TI-1
A/A* P/E
E P A
E P A
TI-2
ap1/P pe1/E
E P A
E P A
TI-3
ap1/P pe1/E
E P A
E P A
TI-4
ap2/P pe2/E
E P A
E P A
TI-5
ap2/P pe2/E
E P A
E P A
NR
P/P E/E
E P A

Supplementary Figure 1: **Overall advancement of tRNAs.**

Translocation of peptidyl- (green) and deacyl-tRNAs (yellow) in the presence of elongation factor 2 (eEF2), shown in red. The mRNA-$tRNA_2$ cargo has been displaced over a distance of approximately 12 Å (measured between respective positions of G34 C1' atoms of peptidyl-tRNA in PRE-H1 and TI-5). Classical positions of reference correspond to tRNA states A/A (from PRE-H1), and P/P and E/E (from NR). On the left, alignment on 25S and, on the right, alignment on the body domain of 18S.

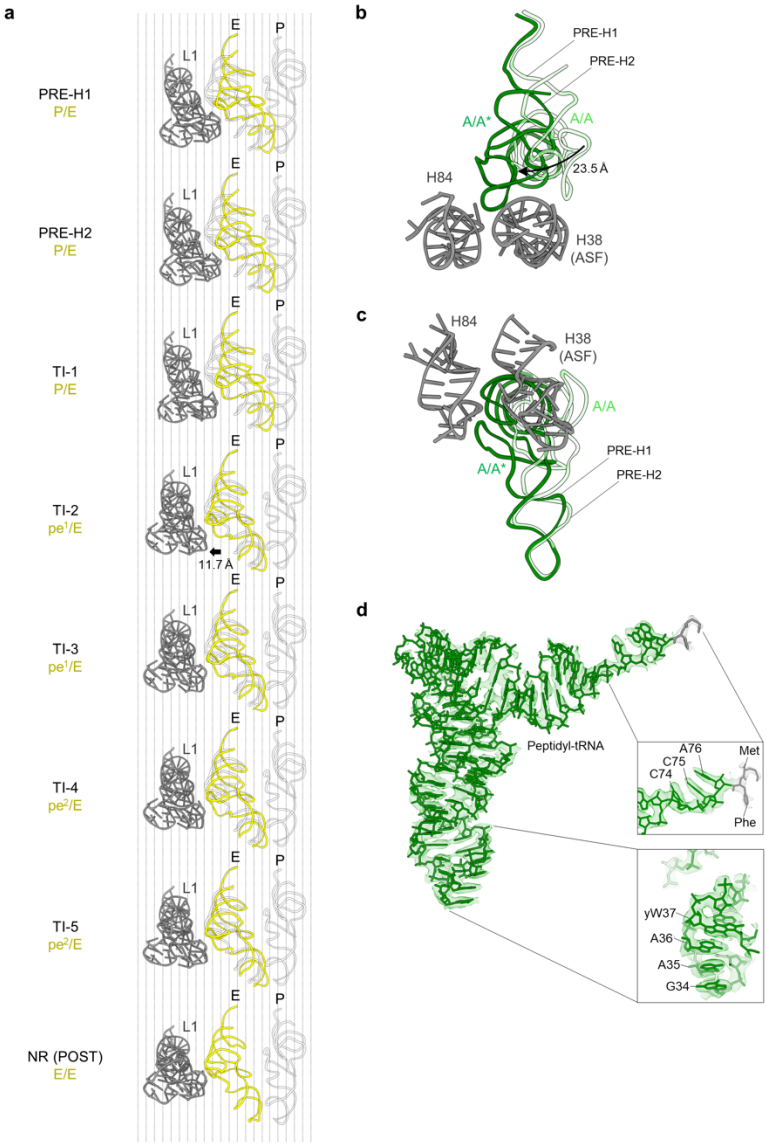
a
PRE-H1
P/E
PRE-H2
P/E
TI-1
P/E
TI-2
pe†/E
TI-3
pe†/E
TI-4
pe‡/E
TI-5
pe‡/E
NR (POST)
E/E
E
P
L1
11.7 Å
b
PRE-H1
PRE-H2
A/A*
A/A
23.5 Å
H84
H38
(ASF)
c
H84
H38
(ASF)
A/A
A/A*
PRE-H1
PRE-H2
d
Peptidyl-tRNA
A76
C75
C74
Met
Phe
yW37
A36
A35
G34

Supplementary Figure 2: **Movement of the L1 stalk and the tRNA elbow shift in pre-translocation-hybrid states.**

a, Advancement of the L1 stalk (grey) associated to translocation of deacyl-tRNA (yellow) towards the E-site. Classical positions of reference correspond to P/P and E/E tRNA states from the NR complex. **b-c**, Inersubunit view, in **b**, and top view, in **c**, of the elbow domain as peptidyl-tRNA advances from A/A (in PRE-H1) to A/A* (PRE-H2). ASF: A-site finger. **d**, Unfiltered, unsharpened density of *S. cerevisiae* fMet-Phe-N-tRNA^{Phe} (e.g. TI-4) contoured at σ = 3.

Complex	40S body domain rotation (°)	40S head domain swiveling (°)	Shoulder closure (°)	Deacyl-tRNA	Peptidyl-tRNA	Translocase module
Non-rotated (NR)	0.0	0.0	0.0	$tRNA^{fMet}$	fMet-$tRNA^{fMet}$	N/A
PRE-H1	11.7	1.0	3.2	$tRNA^{fMet}$	fMet-Phe-N-$tRNA^{Phe}$	N/A
PRE-H2	11.5	1.0	2.9	$tRNA^{fMet}$	fMet-Phe-N-$tRNA^{Phe}$	N/A
TI-1	10.8	1.0	2.2	$tRNA^{fMet}$	fMet-Phe-N-$tRNA^{Phe}$	eEF2·GMPPCP·sordarin
TI-1*	10.2	2.0	1.4	$tRNA^{fMet}$	fMet-Phe-N-$tRNA^{Phe}$	eEF2·GMPPCP
TI-2	4.0	18.1	1.8	$tRNA^{fMet}$	fMet-Phe-N-$tRNA^{Phe}$	eEF2·GDP·sordarin
TI-3	3.3	18.1	2.3	$tRNA^{fMet}$	fMet-Phe-N-$tRNA^{Phe}$	eEF2·GMPPCP·sordarin
TI-4	0.9	19.7	0.6	$tRNA^{fMet}$	fMet-Phe-N-$tRNA^{Phe}$	eEF2·GDP·Pi·sordarin
TI-4*[1]	0.9	18.9	0.6	$tRNA^{fMet}$	fMet-Phe-N-$tRNA^{Phe}$	eEF2·GMPPCP
TI-5	0.4	19.8	0.2	$tRNA^{fMet}$	fMet-Phe-N-$tRNA^{Phe}$	eEF2·GDP·sordarin

[1] Low signal for the $tRNA_D$-mRNA module

Supplementary Table 1: Overview of solved complexes, rotational motions of SSU domains, ribosomal ligands and eEF2 binding counterparts.

Supplementary Video 1: Conformational changes of the eukaryotic ribosome during tRNA translocation.

The video recapitulates mRNA-tRNA progression through the ribosome starting from pre-translocation hybrid intermediates (PRE-H1 to PRE-H2), eEF2 recruitment (TI-1) and accommodation (TI-2). The complex then undergoes sequential transitions from TI-2 to TI-5, resulting in the POST state. Peptidyl-tRNA in shown in green, deacyl-tRNA in violet, eEF2 in red, LSU (60S) is depicted in light-blue, SSU (40S) head and body domains in light brown and orange, respectively.

Supplementary Video 2: eEF2-assisted advancement of transfer RNAs during translocation on the eukaryotic ribosome.

Morphing of unfiltered, unsharpened cryo-EM maps reveals structural dynamics of the mRNA-$tRNA_2$ module advancement during translocation. The sequence reflects progressive transitions between hybrid (PRE-H1, PRE-H2 and TI-1) and chimeric states (TI-2 to TI-5), yielding the classical POST state. Peptidyl-tRNA is shown in green, deacyl-tRNA in yellow, eEF2 in red and mRNA in magenta.

Supplementary Video 3: Accuracy of ribosomal translocation in Eukaryotes: Opening of the decoding center and role of diphthamide.

The video shows an intricated network of interactions on the atomic level, which maintains the mRNA translational reading frame during translocation. It also shows the locked conformation of the eukaryotic decoding center, which undergoes unlocking as domain IV protrudes into the A-site following the accommodation of eEF2 on the ribosome. Peptidyl-$tRNA^{Phe}$ (green), deacyl-$tRNA^{fMet}$ (violet), mRNA (magenta), SSU (light-brown), uS12 (orange), potassium ion (dark violet), eEF2 (red). PDB ID 7OSM corresponds to the crystal structure of the early intermediate translocation complex.

Supplementary Video 4: Role of elongation factor 2 (eEF2) during eukaryotic ribosome translocation.

Interface view of the SSU (40S) illustrates SSU rotation and head domain swiveling during mRNA-$tRNA_2$ translocation. Progressive advancement of ASLs of peptidyl-tRNA (green) and

deacyl-tRNA (violet) is shown from early hybrid to late chimeric states of translocation as the ligands proceed to their classical positions in the POST state. eEF2 contributes to translocation most likely by preventing reverse rotation of the SSU head domain, acting as a molecular "doorstop". The head of SSU (40S) is shown in orange, SSU body in light-brown, and eEF2 in red.

Supplementary video 5: Role of the 1-methyl-3-α-amino-α-carboxyl-propyl pseudouridine 1191 ($m^1acp^3\Psi$1191) hypermodification in eukaryotic ribosome translocation.

The heavily modified uridine, found in the hairpin loop of the universally conserved helix 31 of 18S rRNA lies at the interface of SSU (40S) head and body domains. During translocation, $m^1acp^3\Psi$1191 acts by repetitively guiding tRNA from P- to E-site.

Supplementary Video 6: Maintenance of the translational reading frame during eukaryotic translocation.

Translocation intermediate 4 (TI-4) is given as an example. Residues of SSU (40S) head and body domains, assisted by residues of eEF2 domain IV including diphthamide, form an extensive network of interactions with codon-anticodon duplexes and maintain the translational reading frame during translocation in Eukaryotes. Peptidyl-tRNA is shown in green, deacyl-tRNA in violet, eEF2 in red, mRNA in magenta, residues of SSU head and body domains are depicted in light brown and orange, respectively, and uS9 is shown in dark blue.